Climate Dynamics (2023) 61:2371–2393
https://doi.org/10.1007/s00382-023-06679-w

Thermohaline patterns of intrinsic Atlantic Multidecadal Variability in MPI-ESM-LR

Davide Zanchettin[1] · Shih-Wei Fang[2] · Myriam Khodri[3] · Nour-Eddine Omrani[4] · Sara Rubinetti[5,6] · Angelo Rubino[1] · Claudia Timmreck[2] · Johann H. Jungclaus[2]

Received: 23 August 2022 / Accepted: 14 January 2023 / Published online: 2 February 2023
© The Author(s), under exclusive licence to Springer-Verlag GmbH Germany, part of Springer Nature 2023

Abstract

A vivid scientific debate exists on the nature of the Atlantic Multidecadal Variability (AMV) as an intrinsic rather than predominantly forced climatic phenomenon, and on the role of ocean circulation. Here, we use a multi-millennial unperturbed control simulation and a Holocene simulation with slow-varying greenhouse gas and orbital forcing performed with the low-resolution version of the Max Planck Institute Earth System Model to illustrate thermohaline conditions associated with twelve events of strong AMV that are comparable, in the surface anomalies, to observations in their amplitudes (~ 0.3 °C) and periods (~ 80 years). The events are associated with recurrent yet spatially diverse same-sign anomalous sea-surface temperature and salinity fields that are substantially symmetric in the warm-to-cold and following cold-to-warm transitions and only partly superpose with the long-term spatial AMV pattern. Subpolar cold-fresh anomalies develop in the deep layers during the peak cold phase of strong AMV events, often in association with subtropical warm-salty anomalies yielding a meridional dipole pattern. The Atlantic meridional overturning circulation (AMOC) robustly weakens during the warm-to-cold transition of a strong AMV event and recovers thereafter, with surface salinity anomalies being potential precursors of such overturning changes. A Holocene simulation with the same model including volcanic forcing can disrupt the intrinsic AMV–AMOC connection as post-eruption periods often feature an AMOC strengthening forced by the volcanically induced surface cooling. Overall, our results support the AMV as a potential intrinsic feature of climate, whose episodic strong anomalous events can display different shades of spatial patterns and timings for the warm-to-cold and subsequent cold-to-warm transitions. Attribution of historical AMV fluctuations thus requires full consideration of the associated surface and subsurface thermohaline conditions and assessing the AMOC–AMV relation.

Keywords Atlantic Multidecadal Variability · Intrinsic ocean variability · Meridional overturning circulation · Paleoclimate simulation · Volcanic forcing

✉ Davide Zanchettin
davidoff@unive.it

1 Department of Environmental Sciences, Informatics and Statistics, University Ca' Foscari of Venice, Via Torino 155, 30172 Mestre, Italy

2 Max-Planck-Institute for Meteorology, Bundesstr. 53, 20146 Hamburg, Germany

3 Laboratoire d'Océanographie et du Climat: Expérimentations et Approches Numériques, Institut Pierre-Simon Laplace, Sorbonne Universités /IRD/CNRS/MNHN, Paris, France

4 Geophysical Institute, University of Bergen and Bjerknes Centre for Climate Research, 7803, 5020 Bergen, Norway

5 Alfred Wegener Institute, Helmholtz Centre for Polar and Marine Research, Bussestraße 24, 27570 Bremerhaven, Germany

6 Alfred Wegener Institute, Helmholtz Centre for Polar and Marine Research, Hafenstraße 43, 25992 List, Sylt, Germany

1 Introduction

Oceanic variability in the North Atlantic is characterized by large multidecadal fluctuations in basin-average sea-surface temperature (SST) as shown by observations (Enfield et al. 2001), proxy-based reconstructions (e.g., Gray et al. 2004; Svendsen et al. 2014; Moore et al. 2017; Waite et al. 2020) and numerical simulations (e.g., Zanchettin et al. 2013, 2014, 2016a; Fang et al. 2021; Oldenburgh et al. 2021). This phenomenon is often referred to as Atlantic Multidecadal Oscillation or, alternatively, Atlantic Multidecadal Variability or AMV (Frajka-Williams et al. 2017). The AMV has important implications for multidecadal variability of Northern Hemisphere regional climates (e.g., Enfield et al. 2001) but has inter-hemispheric implications as well (e.g., Knight et al. 2006; Li et al. 2014; Zanchettin et al. 2016b; Ruprich-Robert et al. 2017; Ruprich-Robert et al. 2021; Hodson et al. 2022). It is also among the key phenomena linked to decadal climate predictability (Martín-Rey et al. 2015; Boer et al. 2016; Frajka-Willams et al. 2017; Omrani et al. 2022).

Despite being essentially associated with the alternation of basin-scale surface warming and cooling phases of the North Atlantic, the AMV has been recognized as a multivariate phenomenon (Yan et al. 2019; Omrani et al. 2022). Observations indicate that AMV fluctuations are linked with analog basin-scale changes in sea-surface salinity (SSS), so that warming corresponds to salinification and cooling to freshening (e.g., Polyakov et al. 2005; Delworth and Zeng 2016; Zhang 2017). The surface imprint of the AMV further corresponds to same-sign fluctuations in the shallow ocean and with opposite-sign fluctuations in the deep ocean for both temperature and salinity (Polyakov et al. 2005). This out-of-phase behavior reflects the thermohaline overturning circulation shaping North Atlantic low-frequency variability. Accordingly, several studies interpreted the AMV as strongly connected with the Atlantic Meridional Overturning Circulation (AMOC), and the associated heat transport into the North Atlantic subpolar gyre region (Delworth and Mann 2000; Knight et al. 2006; Zanchettin et al. 2014; Zhang et al. 2016, 2017; Li et al. 2020; Oelsmann et al. 2020; Hand et al. 2020; Fang et al. 2021; Lai et al. 2022; Omrani et al. 2022). Also, in the North Atlantic subpolar gyre region, recirculation of salinity anomalies from Arctic freshwater export may trigger multidecadal and longer AMOC variability (Jungclaus et al. 2005; Dima and Lohmann 2007; Jiang et al. 2021; Meccia et al. 2022), and therefore be part of the AMV. Internal oceanic mechanisms responsible for decadal and bidecadal North Atlantic variability associated with the development of large-scale baroclinic instabilities (e.g., Arzel et al. 2018; Gastineau et al. 2018) may also be relevant for oceanic circulation on longer timescales, including the AMV.

However, the internal AMV mechanism may depend on model specificities (Lai et al. 2022) and the role of the AMOC and oceanic circulation in general in driving the AMV has been questioned by some authors (Clement et al. 2015, 2016) and some recent model studies highlight the role of external forcing through ocean–atmosphere surface processes for the AMV (e.g., Bellucci et al. 2017; Murphy et al. 2017; Bellomo et al. 2018).

Attribution of the AMV is thus subject to vivid scientific debate. The twentieth century AMV evolution stems from the competition between internal dynamics and external forcing, predominantly in the form of tropospheric aerosols (e.g., Knight 2009; Medhaug and Furevik 2011; Booth et al. 2012; Zhang et al. 2013; Bellomo et al. 2018; Watanabe and Tatebe 2019). For the preindustrial period of the last millennium, when anthropogenic forcing is minimal, proxy-based reconstructions, re-analyses and paleoclimate model simulations mostly link the externally forced AMV to volcanic activity (e.g., Otterå et al. 2010; Winter et al. 2015; Birkel et al. 2018; Mann et al. 2021; Fang et al. 2021; Klavans et al. 2022). Accordingly, the pacing of major volcanic eruptions during the last millennium matching the typical timescale of the AMV can explain the emergence of AMV-like fluctuations in transient paleoclimate simulations (Mann et al. 2021). However, a separation of AMV from a multi-model paleoclimate simulation ensemble in its internal component—due to intrinsic dynamics and linked with the AMOC—and external component—linked with coherent SST changes across all basins of the World Ocean—reveals that the internal component of the AMV is unaffected by volcanic activity (Fang et al. 2021). Also, according to a recent assessment, the volcanically driven component contributed to about one third of the preindustrial AMV variance (Klavans et al. 2022). Physical understanding of the AMV during the preindustrial period is also complicated by the variety of behaviors seen in millennial-scale unperturbed and transient paleoclimate simulations, including non-stationarity in the amplitude of multidecadal basin-scale North Atlantic SST signals (e.g., Zanchettin et al. 2010, 2013) and variable relationships with large-scale atmospheric circulation features and inter-basin interactions (e.g., Wu et al. 2011; Zanchettin et al. 2014, 2016a; Meehl et al. 2021). Changes in the mean climate state may also affect the AMV, as suggested by Moore et al. (2017). Therefore, multiple AMV mechanisms may exist, and different mechanisms may be active or dominant under different circumstances.

With this contribution, we characterize the oceanic contribution to the AMV simulated by the Earth system model developed at the Max Planck Institute for Meteorology in its low-resolution configuration (MPI-ESM-LR) by focusing on the associated evolution and spatial patterns of the salinity and temperature fields at the sea surface and in the

shallow and deep ocean. We focus on an unperturbed millennial-scale simulation and a 6000-year Holocene simulation under slow-varying forcing performed with MPI-ESM-LR, and therefore focus on internal dynamics. We track the horizontal and vertical propagation of temperature and salinity anomalies during twelve AMV events that are comparable with historical AMV observations regarding the amplitude and timescale of the fluctuations. We highlight differences between the events regarding the spatial pattern of North Atlantic SST and SSS, AMOC and subpolar gyre circulation, therefore supporting the multifaceted nature of the AMV. In addition, we use MPI-ESM-LR transient simulations covering the Common Era (from year -150 to 1850 CE) to discuss how the simulated AMV properties change under the effects of different combinations of natural forcing.

2 Data and methods

2.1 Earth system model

MPI-ESM is composed of the atmospheric general circulation model ECHAM6 (Stevens et al. 2013), the ocean-sea ice model MPIOM (Jungclaus et al. 2013), the land component JSBACH (Reick et al. 2013), which is directly coupled to ECHAM6, and the ocean biogeochemistry model HAMOCC (Ilyina et al. 2013), which is directly coupled to MPIOM. In MPI-ESM-LR, ECHAM6.3 is run at T63L47, corresponding to a horizontal resolution of approximately 200 km on a Gaussian grid, while MPIOM is run with a nominal horizontal resolution of 1.5° and 40 vertical levels. ECHAM6.3 includes modifications of the convective mass flux, convective detrainment and turbulent transfer, the fractional cloud cover and a new representation of radiative transfer with respect to the version used in the Coupled Model Intercomparison Project phase 5 (CMIP5) (Stevens et al. 2013), while MPIOM remained largely unchanged with respect to the CMIP5 version of MPI-ESM (Jungclaus et al. 2013). A detailed description of parameterizations for mixing and diffusion in MPIOM is provided by Marsland et al. (2003) and Jungclaus et al. (2013). The MPI-ESM-LR version used here differs from the CMIP6 version of MPI-ESM (Mauritsen et al. 2019), but it is overall closer to it than to the previous CMIP5 version (Giorgetta et al. 2013).

MPI-ESM-LR has been extensively employed in studies of intrinsic climate dynamics in the framework of the Max Planck Institute Grand Ensemble (MPI-GE, Maher et al. 2019) and in paleoclimate applications (Bader et al. 2020; Dallmeyer et al. 2021). Moreover, the CMIP5 and CMIP6 versions of MPI-ESM have been extensively validated in the context of multi-model ensemble analyses for paleoclimatology and in simulation-proxy comparative assessments (Jungclaus et al. 2014; Moreno-Chamarro et al. 2015, 2017a, b), including studies with explicit focus on the AMV (Zanchettin et al. 2014, 2016a,b; Oelsmann et al. 2020; Fang et al. 2021; Omrani et al. 2022).

2.2 Simulations

Three simulations are considered, which allows us to compare intrinsic and naturally forced characteristics of the AMV. The first simulation is a 2000-year unperturbed pre-industrial control simulation (piControl), where external forcing is kept constant at year 1850 levels. The simulation expresses intrinsic climate variability of MPI-ESM-LR, which arises from spontaneous instabilities generated in the coupled climate system. The second and third simulations are Holocene transient simulations performed with different combinations of external natural forcing: one considers only orbital changes in insolation and changes in natural pre-industrial greenhouse gas concentrations and spans from years −6000 to 1850 (Holo_GHG-ORB); the other also includes volcanic forcing and changes in solar activity and in land use (Holo_volc) (Dallmeyer et al. 2021). For Holo_volc, we only use the last 2000-year period of the simulation, where the prescribed external forcing follows the protocol for the "past2k" experiment of the Paleoclimate Model Intercomparison Project phase 4 (Jungclaus et al. 2017). Major volcanic eruptions are identified from the eVolv2k volcanic history, including events on the following years: 540, 574, 682, 939, 1108, 1182, 1230, 1257, 1286, 1345, 1453, 1600, 1640, 1695, 1783 and 1815. The eruption dates are taken from Table S3 of Toohey and Sigl (2017) excluding eruptions too closely followed by another eruption.

2.3 Observational data

Gridded SST observational data for the period 1870–2019 are obtained from the Hadley Centre Sea Ice and Sea Surface Temperature data set (HadISST1, Rayner et al. 2003). We also use the unsmoothed 1856-present monthly time series of the Atlantic Multidecadal Oscillation index calculated at NOAA PSL based on the Kaplan SST V2 dataset, available at the url: https://psl.noaa.gov/data/timeseries/AMO/ (Enfield et al. 2001). Based on this index, two periods are defined which start in 1865 (event E1) and 1931 (event E2), each encompassing a ~ 80-year long warm-to-cold-to-warm AMV event. For each observed event, the warm phases are defined as 17-year periods covering years 6th–22nd (initial warm phase) and 69th–85th (final warm phase) from the start year of the event; the cold phase is defined as the 17-year period covering years 41st–57th from the start year

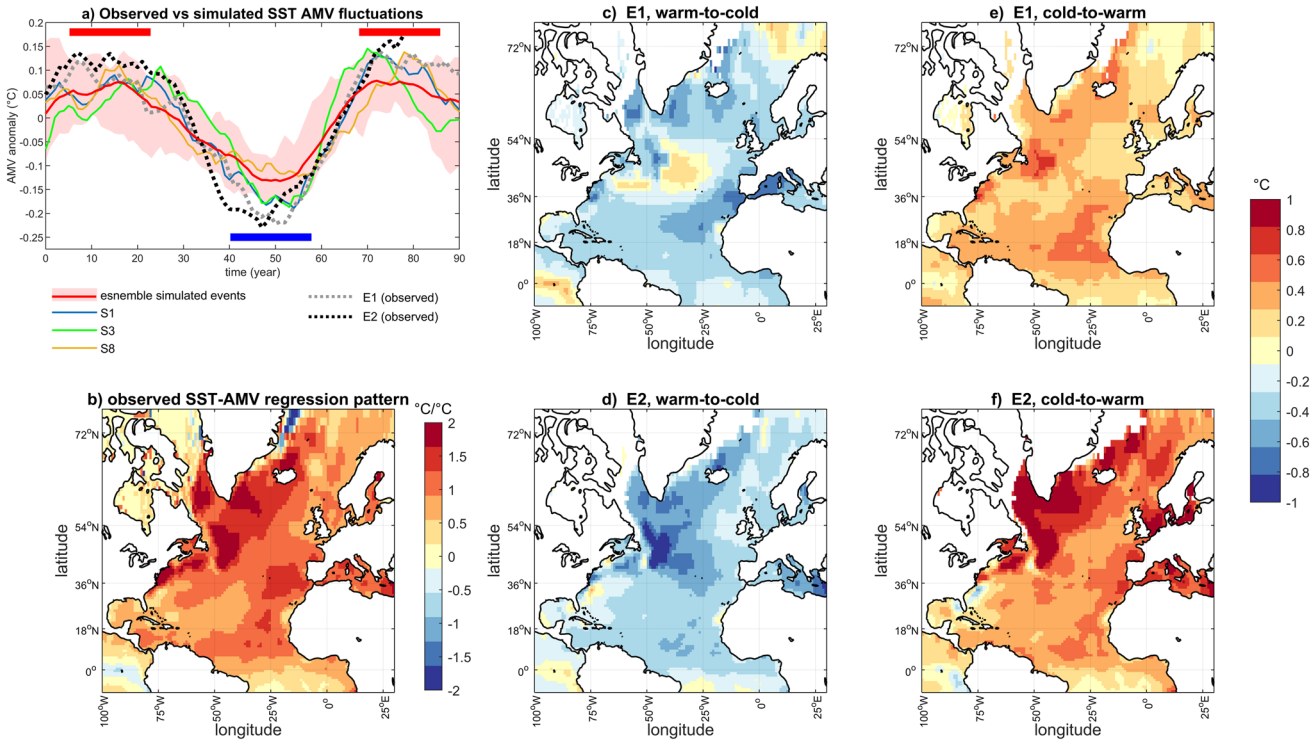

Fig. 1 **a** Comparison between observed and simulated AMV fluctuations in North Atlantic average annual-mean sea-surface temperature (SST). Shown are superposed epochs of fluctuations in the observed AMV index (Kaplan SST AMO, grey and black dashed lines, events E1 and E2, respectively) and in the $TAMV_{surf}$ index during the twelve simulated events detected in piControl and Holo_GHG-ORB (red shading and line: ensemble envelope and mean of the twelve events; blue, green and orange lines: selected individual events), smoothed with a 21-year running mean. The horizontal bars illustrate the approximate occurrence of peak warm (red) and cold (blue) phases of each fluctuation used for the calculation of anomalies; **b** Observed regression pattern of the AMV on SST; **c**–**f** Observed sea-surface temperature anomalies calculated for the warm-to-cold (average during cold phase minus average during initial warm phase) and the following cold-to-warm (average during final warm phase minus average during cold phase) transitions of the two observed AMV fluctuations (events E1 and E2). See Sect. 3.2 for definition of warm and cold phases

of the event (see red and blue bars in Fig. 1a). The initial warm phase of E2 overlaps with the final warm phase of E1.

2.4 Indices

AMV indices are defined for temperature (TAMV) and salinity (SAMV) by spatially averaging monthly data covering the domain between 80° and 0° W longitude and 0°–60° N latitude, excluding the interior of the Labrador Sea to avoid influences by sea ice as in Zanchettin et al. (2016a, b). Indices are calculated for all model vertical levels, with a focus on sea-surface fields ($TAMV_{surf}$ and $SAMV_{surf}$) and fields at shallow (310 m) and deep (2080 m) depths ($TAMV_{310/2080}$ and $SAMV_{310/2080}$, for temperature and salinity, respectively). $TAMV_{surf}$ corresponds to the classical AMV index.

The Holo_GHG-ORB simulation contains multi-millennial trend in AMV indices, which is estimated, for $TAMV_{surf}$, in 0.025–0.028 °C/millennium. The full-period linear trend is removed from all used data before analyses. An AMOC index is defined as the zonally integrated vertical mass streamfunction in the North Atlantic at 26.5° N and 1020 m depth. An index describing the variable strength of the North Atlantic subpolar gyre is defined as the yearly time series of minima of the annual mean barotropic mass streamfunction simulated in the subpolar gyre core region. In this study, the terms interdecadal and multidecadal refer to timescales of 20–50 years and 50–90 years, respectively.

The Gibbs SeaWater (GSW) Oceanographic Toolbox of TEOS-10 is used to calculate partial derivatives of density with respect to SST and SSS, i.e., the contribution of temperature and salinity changes to density changes.

2.5 Statistical analysis

The statistical significance of correlations is computed accounting for the effective degrees of freedom of the series following Dawdy and Matalas (1964). Wavelet analysis is performed using the toolbox by Torrence and Compo (1998) and Grinsted et al. (2004). The Morlet function ($w_0 = 6$) is used as the mother wavelet.

Episodes of strong AMV fluctuations are identified in piControl and Holo_GHG-ORB based on a statistical comparison between simulated and observed $TAMV_{surf}$ indices. Specifically, these refer to 90-year periods along the simulations when statistical correlation between anomalies of simulated and observed smoothed indices (17-year running mean) exceeds the value of 0.8 and the root mean square is minimal. The considered 90-year period allows to fully encompass the warm-to-cold-to-warm transitions that characterize the observed events. In analogy with the definition of warm and cold phases in AMV observations, changes in thermohaline properties during the selected events of strong warm-to-cold-to-warm fluctuations of simulated AMV are calculated, for each event, as differences between the averages of 17-year periods centered around consecutive warm and cold states (cold minus warm state, for the initial cooling) and between the averages of 17-year periods centered around the cold state and the following warm state (warm minus cold state, for the final warming). The center of the cold and warm states corresponds to the year of the coldest and warmest smoothed AMV index, respectively.

For observations, two AMV fluctuations are considered, that start in years 1865 and 1931, which accordingly yields the following warm and cold states (see Sect. 3.1). For the first event: 1870–1886 warm, 1905–1921 cold, 1933–1949 warm; for the second event: 1936–1952 warm, 1971–1987 cold, 1999–2015 warm.

Only local differences that exceed the 10–90 percentile range of the signal obtained from an analysis over the whole length of the considered simulations are considered as statistically significant, except where stated otherwise. Data are linearly detrended during each simulated event to remove longer-term variations, which is especially relevant for deep ocean layers.

Spatial patterns are compared using cell-area weighted spatial correlation and root mean square error (rmse) for the region 75–0° W longitude and 0–65° N latitude. Simulated patters are interpolated to the observational grid before calculation of spatial correlations and rmse. For comparison between AMV regression patterns and warm-to-cold anomalies, the latter are multiplied by −1 before computation of spatial correlation and rmse.

3 Results

3.1 Observed AMV fluctuations and associated spatial patterns

Figure 1 illustrates observed characteristics of the AMV that serve as a basis for the analysis of its simulated features. Two events can be recognized in the time series of the observed AMV index, which is available since the mid-nineteenth century. Each event includes a warm-to-cold and a subsequent cold-to-warm transition of similar amplitude (about 0.3 °C) and duration, each lasting 40–50 years, hence yielding a warm-to-cold-to-warm AMV fluctuation of 80–90 years. The two events are named E1 and E2 and are illustrated in Fig. 1a. The SST anomalies calculated for E1 and E2 share basin-scale tendencies, i.e., broad cooling (left panels) followed by broad warming (right panels).

The events display remarkable differences in the regions where the largest anomalies occur. In the warm-to-cold transition, E1 enhances cooling in the Canary current branch of the subtropical gyre and in the interior of the Labrador Sea, with a slight warming along the Gulf Stream (Fig. 1c). In contrast, in the warm-to-cold transition E2 features basin-scale cooling with the largest anomalies along the Gulf Stream, especially its separation region and in the eastern subpolar gyre (Fig. 1d). Spatial correlation between the AMV regression pattern and the warm-to-cold anomaly pattern in E1 (E2) is 0.11 (0.80), with an rmse of 0.80 (0.70). The following cold-to-warm transitions mirror to a large extent the cooling phases, suggesting an overall symmetry along each fluctuation, which is less evident in E1 (Fig. 1e) compared to E2 (Fig. 1f). The cold-to-warm anomaly pattern in E1 (E2) yields a spatial correlation of 0.46 (0.80) and rmse of 0.77 (0.63) when compared with the AMV regression pattern. Overall, E2 superposes well on the regression pattern of the observed AMV index on North Atlantic SSTs (Fig. 1b), whereas E1 does not especially in the initial warm-to-cold transition. The coarser in-situ data used in the HadISST dataset during E1 with respect to E2 might contribute to explain the differences. Otherwise, the much stronger spatial correlations in E2 compared to E1 may suggest that the regression pattern highlights the forced pattern and does not fully account for the internal component of AMV. Further, the spatial differences may highlight differences in the external forcing of AMV and/or different contributions, in E1 and E2, of intrinsic climate variability. Nonetheless, observations point to a variety of cooling and warming patterns associated with AMV fluctuations, that are characterized by large anomalies over regions of the basin that do not emerge as important in the AMV regression pattern.

In the following, observations are used as a target to identify periods of simulated strong AMV fluctuations in piControl and Holo_GHG-ORB to (1) determine the potential for intrinsic climate variability alone to produce AMV that is, at the surface, comparable with historically observed events (affected by external forcing agents, including anthropogenic ones) in terms of magnitude and duration of the associated fluctuations, (2) identify common features and specificities of intrinsic strong AMV fluctuations, and (3) determine whether and how natural external forcing can modify the thermohaline structure of the AMV. Due to our experimental setup, anthropogenic forcing of AMV, including for instance

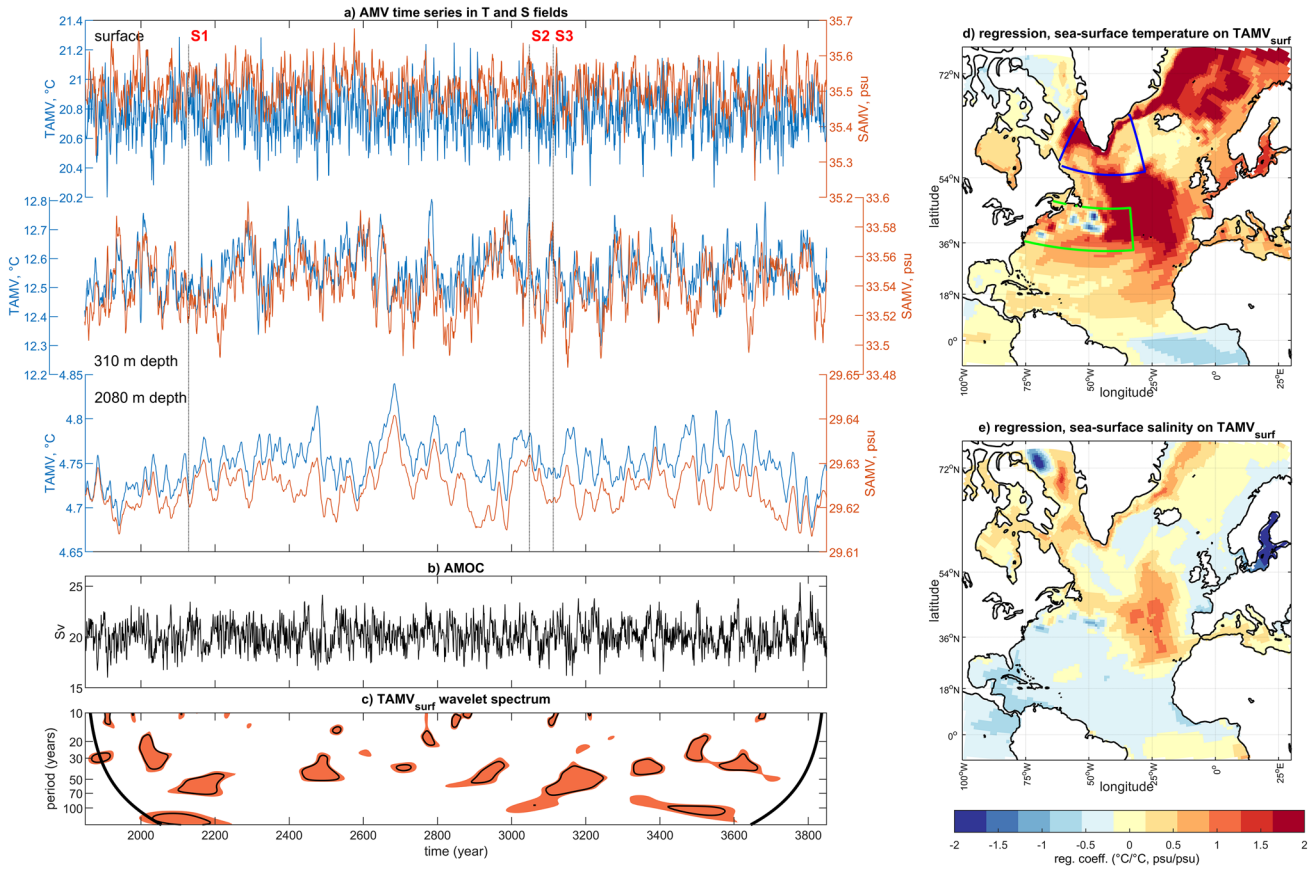

Fig. 2 Intrinsic basin-scale thermohaline variability in the North Atlantic simulated by MPI-ESM-LR in the piControl simulation. **a** Annual time series of spatially averaged temperature and salinity over the AMV domain (0–60° N, 0–80° W) (TAMV and SAMV indices, respectively) at selected depths; **b** Annual time series of the AMOC; **c** wavelet spectrum of the TAMV$_{surf}$ index. Shown are regions of the time–frequency space where the wavelet spectrum is significant at 90% (red shading) and 95% (black contour) confidence against a lag-1 autoregressive process. The thick line indicates the cone of influence where edge effects occur; **d**, **e** regression patterns of North Atlantic SST and SSS with the TAMV$_{surf}$ index for data smoothed with a 21-year running average. The blue and green line contours indicate boxes used for the calculation of thermohaline properties in the subpolar gyre and Gulf Stream regions, respectively. The beginning of the three events of strong AMV fluctuations considered in this analysis are indicated by S1–S3 and by the vertical dashed lines on top of **a**

tropospheric aerosol that was potentially relevant for the historical AMV evolution, is not considered.

3.2 Intrinsic AMV variability in basin-average temperature and salinity

Figure 2 summarizes the simulated intrinsic variability of basin-average North Atlantic seawater temperature and salinity from piControl. Large multidecadal fluctuations are apparent in TAMV and SAMV both at the surface and in the ocean interior (Fig. 2a). TAMV$_{surf}$ anomalies are associated with same-sign fluctuations across the North Atlantic (Fig. 2d) with a regression pattern highlighting the mid-latitude and subpolar central North Atlantic and regions affected by sea-ice dynamics. The latter regions, including the Labrador Sea and the Norwegian and Greenland Seas, are outside the domain used for the calculation of the AMV indices. Both simulated and observed AMV patterns show prominent warming along the mid-latitudes, but the position of the largest SST variations does not overlap (it is more central in the simulated and in the western part in the observed pattern), yielding a spatial correlation of 0.38 and rmse of 0.66. The regression pattern between the SSS field and TAMV$_{surf}$ superposes well on the regression pattern between SST and TAMV$_{surf}$, and it entails an extensive positive signature over the mid and subpolar latitudes (Fig. 2e). The weaker correlations over the tropics and along the Gulf Stream, together with the strong positive correlations toward the Arctic Ocean and especially along the Greenland current, suggest that TAMV$_{surf}$ variability is also linked to modulation of the freshwater budget in the subpolar gyre linked to sea-ice dynamics. Analogously to Fig. 2, Fig. 3 illustrates the simulated variability of basin-average North Atlantic seawater temperature and salinity from Holo_GHG-ORB.

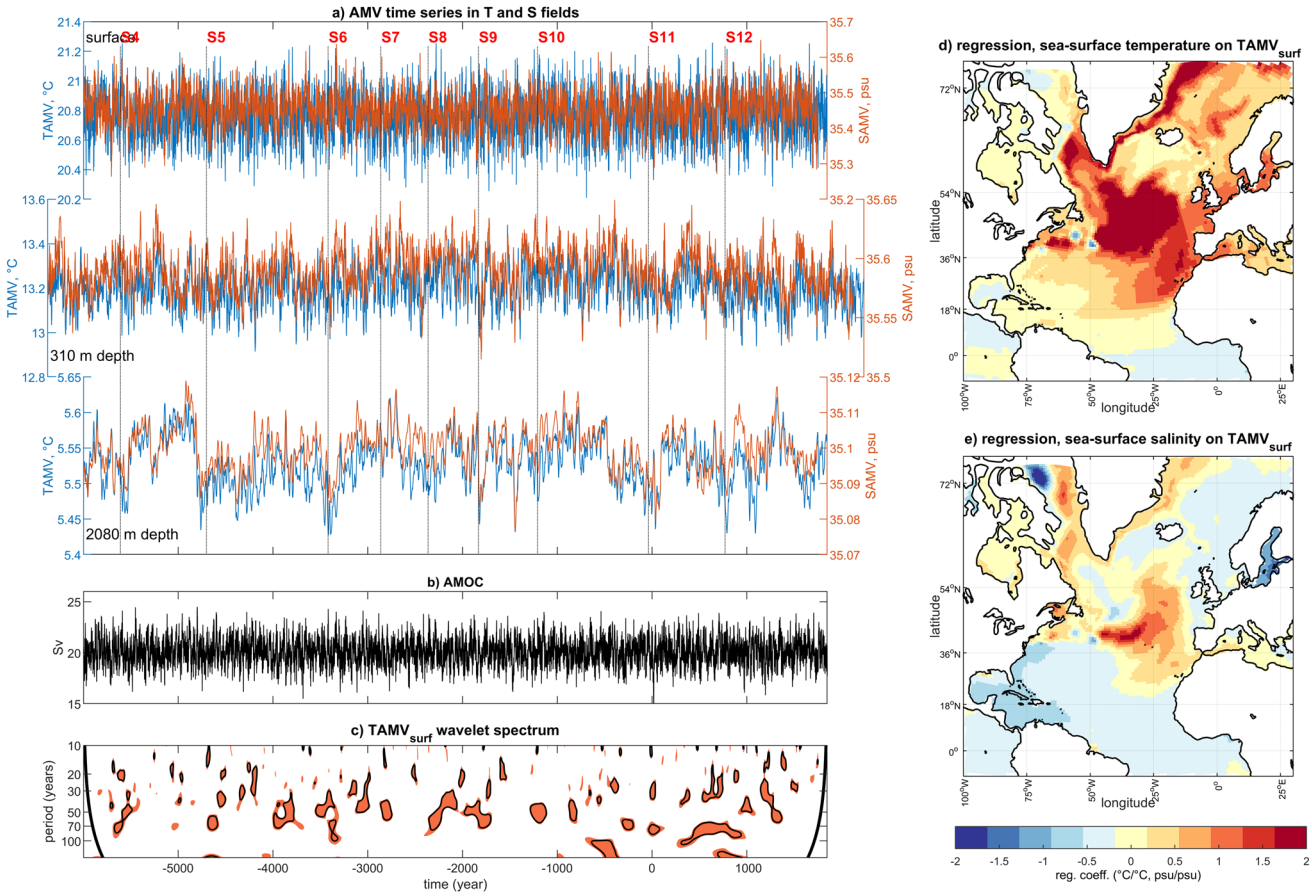

Fig. 3 Basin-scale thermohaline variability in the North Atlantic simulated by MPI-ESM-LR in the Holo_GHG-ORB simulation. Representation as Fig. 2

Temporal and spatial AMV characteristics for this simulation are remarkably consistent with those under unperturbed climate conditions (spatial correlation and rmse between AMV patterns in panels d of Figs. 2 and 3 are 0.91 and 0.33, respectively), which suggests that intrinsic AMV-like thermohaline variability remains substantially unaltered under slow-varying orbital and greenhouse gas forcing.

Significant regions in the multidecadal wavelet spectrum of $TAMV_{surf}$ in piControl (Fig. 2c) and Holo_GHG-ORB (Fig. 3c) reveal numerous intermittent periods of strong multidecadal variability. The Holo_GHG-ORB simulation demonstrates that episodic strong AMV fluctuations can occur throughout a simulated period of almost 8000 years, with a few events per millennium, supporting the idea that the AMV is a robust feature of simulated climate variability. Twelve periods of strong AMV fluctuations are detected (see methods), that initiate around simulation years 2129, 3048 and 3112 in piControl, and around simulation years −4610, −3702, −2419, −1863, −1364, −833, −209, 962 and 1770 CE in Holo_GHG-ORB. The second and third events in piControl are consecutive, and thus define a period including two consecutive warm-to-cold-to-warm AMV fluctuations like the observed AMV events. The ensemble of twelve simulated events of strong AMV, hereafter referred to as S1–S12, are illustrated in Fig. 1a, where they are compared with the two observed events E1 and E2. Three events are selected to illustrate the diversity of simulated strong AMV fluctuations: Events S1 and S3 from piControl superpose very well on the observed events concerning magnitude and duration of the anomalies (Fig. 1a); S8 from Holo_GHG-ORB lasts longer and is weaker than observations. Results from the main analyses on all individual events are illustrated in the supplementary material. Overall, all simulated events compare very well with observed events, especially in the warm-to-cold transition.

Figure 4 illustrates the evolution of basin-average depth-resolved temperature and salt anomalies along the ensemble mean of the twelve simulated events (top panels) and along the individual selected events S1, S3 and S8. There is a remarkable symmetry between the ensemble mean temperature and salinity anomalies near the surface, with significant anomalies reaching typically depths around 200 m, i.e., throughout the climatological mixed layer. There is no robust penetration of surface anomalies towards deeper

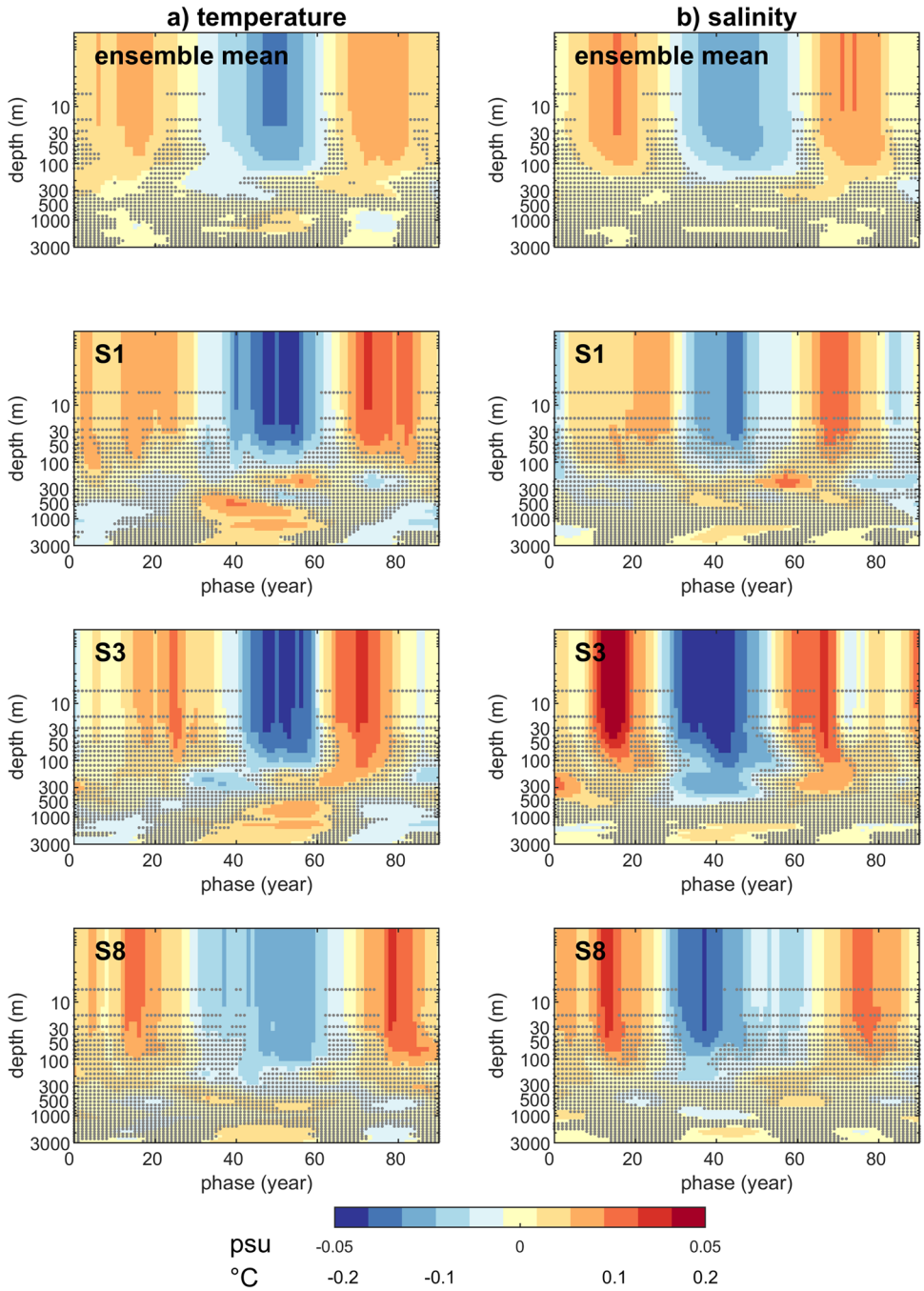

Fig. 4 Time-depth evolution of North Atlantic basin-average seawater temperature (**a**) and salinity (**b**) anomalies during selected simulated AMV events. Top: ensemble mean of twelve events; bottom: three selected events. On top panels, grey dots illustrate grid points where the 25–75 percentile range of ensemble members spans the value of zero, i.e., where the ensemble members disagree on the sign of the anomaly. On bottom panels, the grey dots illustrate grid points where the anomalies do not exceed the 10–90 percentile range obtained from a full-period analysis of piControl

ocean layers: Events S1, S3 and S8 demonstrate that, in individual events of strong AMV fluctuations, thermohaline anomalies around 200–500 m depth are patchy and can be out of phase with the near-surface and deep anomalies (see, e.g., S3 and S8). However, most events agree on the development of temperature anomalies at depths greater than 500 m that have opposite sign with respect to near-surface temperature anomalies.

Considering the whole piControl simulation, coherent fluctuations characterize variability in both $TAMV_{surf}$ and $SAMV_{surf}$ (Fig. 2a), which is confirmed by the significant full-period correlation between both indices, with salinity leading temperature variations by 1 year (Fig. 5a). The subsurface and the deep North Atlantic Ocean both display significant multidecadal thermohaline variability, typically with a rough co-phase between salinity and temperature anomalies (Fig. 2a). Full-period cross-correlations between $TAMV_{surf}$ and $TAMV_{310/2080}$ and $SAMV_{310/2080}$ indices yield wavelike profiles reaching significant peak values corresponding to lagged relationships between the indices

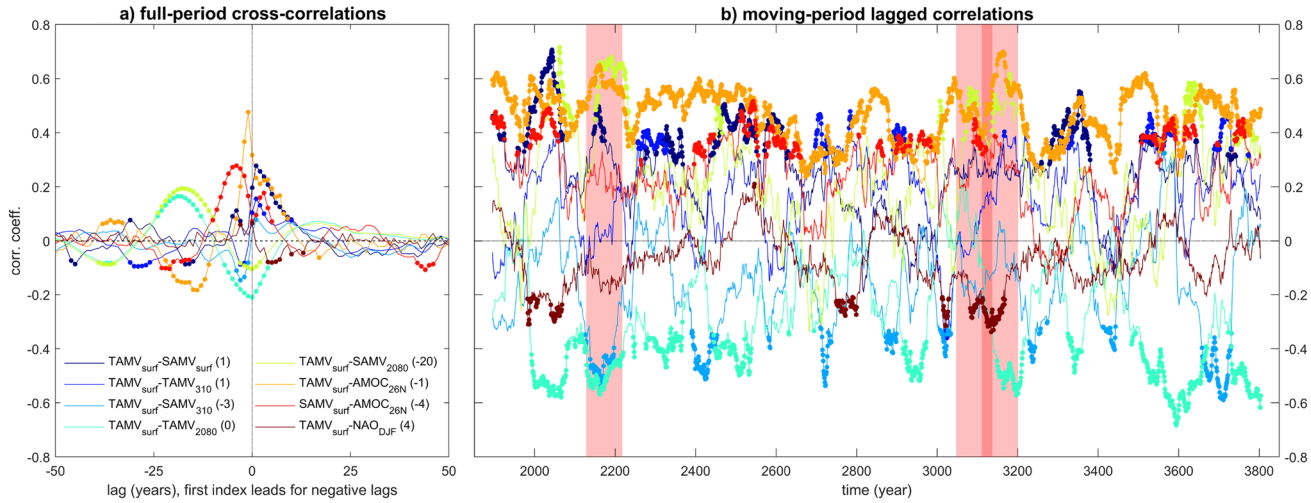

Fig. 5 Correlation across indices describing North Atlantic oceanic variability in piControl. **a** Full-period cross-correlations between annual paired indices. The numbers in brackets in the legend indicate the lag at which the absolute value of the cross-correlation is maximum for each pair of variables; **b** moving-window correlations, with window set to 91 years and for lags as reported in parentheses in the legend. Dots mark correlations significant at 95% confidence accounting for serial correlation in the indices. The red bands in **b** indicate the simulated events S1–S3 of strong AMV

(Fig. 5a). For instance, TAMV$_{surf}$ lags TAMV$_{310}$ by one year while it leads SAMV$_{310}$ by 3 years. Despite significant, the full-period correlation values are small (below 0.2 in absolute value) and indicative of a negligible amount of shared variance between variables.

There is also an antiphase relation between TAMV$_{surf}$ and deep anomalies, seen as significant negative lag-0 correlations with both TAMV$_{2080}$ and SAMV$_{2080}$; for both deep indices positive correlations are found when TAMV$_{surf}$ leads by about two decades, with even stronger magnitude compared to the lag-0 anticorrelation for SAMV$_{2080}$. The lag-0 correlations between surface and interior ocean thermohaline variability are explained by the tight connection between both TAMV$_{surf}$ and SAMV$_{surf}$ with the AMOC (Fig. 2b) as seen by significant full-period cross-correlations, indicating that the AMOC lags TAMV$_{surf}$ by 1–2 years and SAMV$_{surf}$ by a few years (Fig. 5a). The lagged correlations suggest that the coupling between surface and deep thermohaline anomalies is associated with an oscillatory behavior, again explainable through AMOC dynamics.

There is, however, substantial variability through time in the strength of the connection between the surface and interior ocean evolutions of temperature and salinity, and between surface anomalies and the AMOC. Moving-window lag-correlations in Fig. 5b show that the full-length significant cross-correlation between temperature and salinity anomalies stems from intermittent periods of strengthened correlation between both variables. The wavelet coherence spectrum in Fig. 6a further shows that, on interdecadal and multidecadal periods, the connection between TAMV$_{surf}$ and SAMV$_{surf}$ is strengthened in correspondence with the events S1-S3. There is a tight multidecadal connection between both variables after year 3600, in correspondence with strong interdecadal TAMV$_{surf}$ variability (Fig. 2c) that, however, does not superpose on observed AMV fluctuations and is not identified as a strong AMV event. Similarly, the connection between surface and interior ocean thermohaline variations can be temporarily strengthened, also in correspondence with S1–S3. This is shown, for instance, by the lagged correlations between TAMV$_{surf}$ and SAMV$_{2080}$: correlations are mostly non-significant and even occasionally negative, but they are significantly positive during events of strong AMV fluctuations (Figs. 5b and 6d). Similarly, events S1 and S3 but not event S2 are associated with a strengthened anti-correlation and wavelet anti-phase between TAMV$_{surf}$ and TAMV$_{2080}$ (Figs. 5b and 6d).

The TAMV$_{surf}$-AMOC wavelet coherence shows that on multidecadal time scales the AMV slightly lags AMOC changes (Fig. 6f), in contrast with indications from the cross-correlation (Fig. 5a) where interannual variability dominates the TAMV$_{surf}$ signal. AMOC and SAMV$_{surf}$ are significantly correlated at lag(4) only intermittently and noticeably so during event S2, while their correlation can otherwise drop to near-zero values (Fig. 5b). Overall, as far as basin-scale surface changes in the North Atlantic are considered, temperature appears to be a more robust covariate of AMOC changes than salinity, although the latter appears occasionally as a precursor of both basin-scale surface temperature and AMOC changes. A separation of surface density anomalies in their temperature and salinity contributions indicates that the former largely dominates the latter (salinity only explains 20–25% of density changes), even in regions where

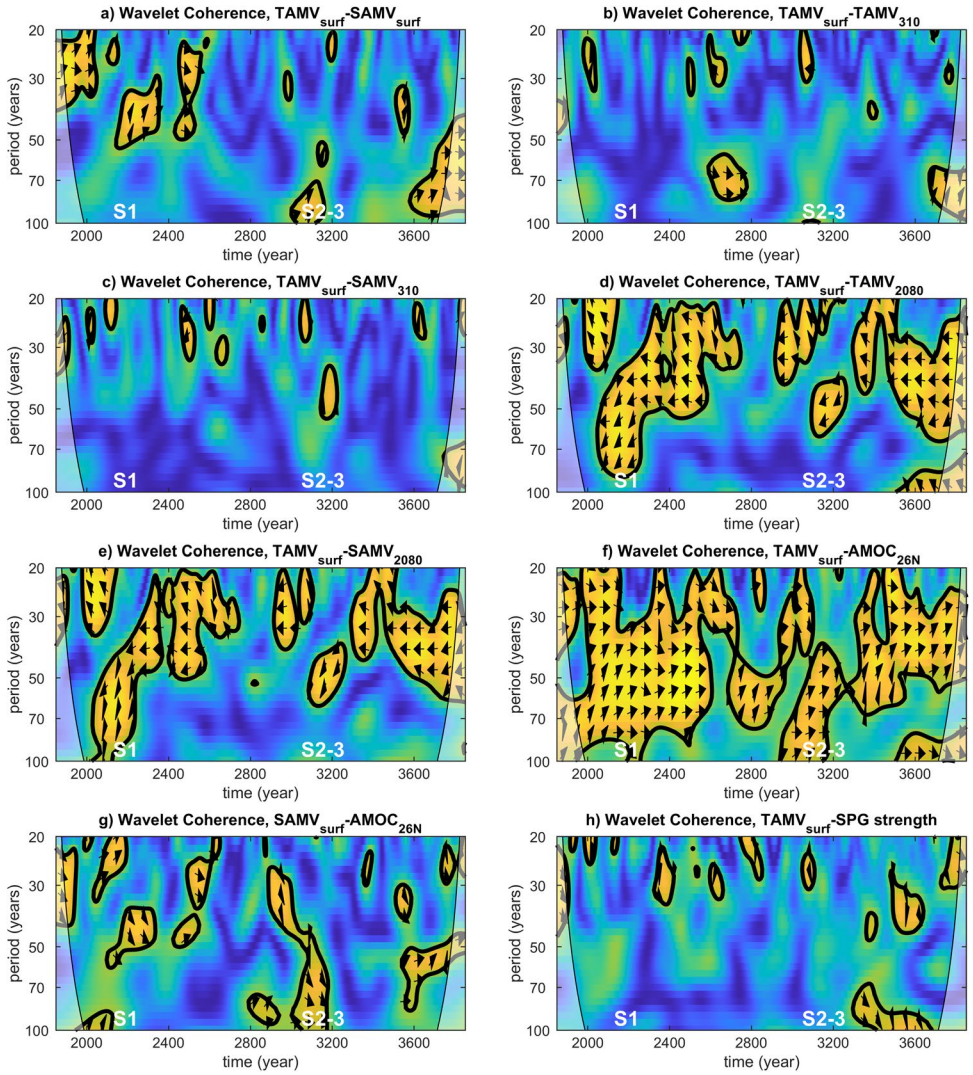

Fig. 6 Wavelet coherence spectra between paired annual indices describing North Atlantic oceanic variability in piControl. Thick contours identify the 5% significance level. Arrows identify the phases (arrows pointing to the right identify co-phase, the first variable leads for clockwise rotation from the co-phase axis). The lightly shaded region indicates where edge effects occur

large salinity anomalies occur during strong AMV fluctuations, due to strong temperature-driven density changes there (see supplementary Fig. S1).

Cross-correlations between surface and deep thermohaline variability and AMOC in Holo_GHG-ORB are consistent with those obtained from the unperturbed simulation: TAMV$_{surf}$ remains anticorrelated with TAMV$_{2080}$ and SAMV$_{2080}$, although there is an overall weaker peak correlation between TAMV$_{surf}$ and AMOC in the transient compared to the unperturbed simulation (Fig. 7a). The rough co-phase between AMOC and TAMV$_{surf}$ emerges as substantially robust over the whole period, with variable strength but almost always significant. The moving-period lagged correlations and wavelet coherence between indices for Holo_GHG-ORB (Fig. 7b–e) confirm the broad alignment of transient and unperturbed conditions regarding the general functioning of simulated North Atlantic thermohaline variability, particularly concerning the strong connection at interdecadal and multidecadal timescales between TAMV$_{surf}$ and AMOC. Possibly, a tighter connection between interdecadal surface variability of basin-scale temperature and salinity compared to unperturbed conditions is established (Fig. 7c). Salinity seems also to become more robustly connected with AMOC under slow-varying transient forcing compared to unperturbed conditions, with a predominance of a significant co-phase between SAMV$_{surf}$ and AMOC at near-centennial time scales seen in the wavelet coherence spectrum (Fig. 7e). This suggests a change in the relative dominance of surface salinity versus surface temperature for AMOC variations from unperturbed to transient conditions.

To better illustrate the tight connection between TAMV$_{surf}$ and AMOC, Fig. 8 illustrates anomalies of the Atlantic meridional overturning streamfunction during the warm-to-cold (left) and following cold-to-warm (right) transitions for the ensemble mean and for the individual events S1, S3 and S8 (see supplementary Figure S2 for all events). Note that the duration of the transitions varies among events between 23 and 52 years for the warm-to-cold transition and between

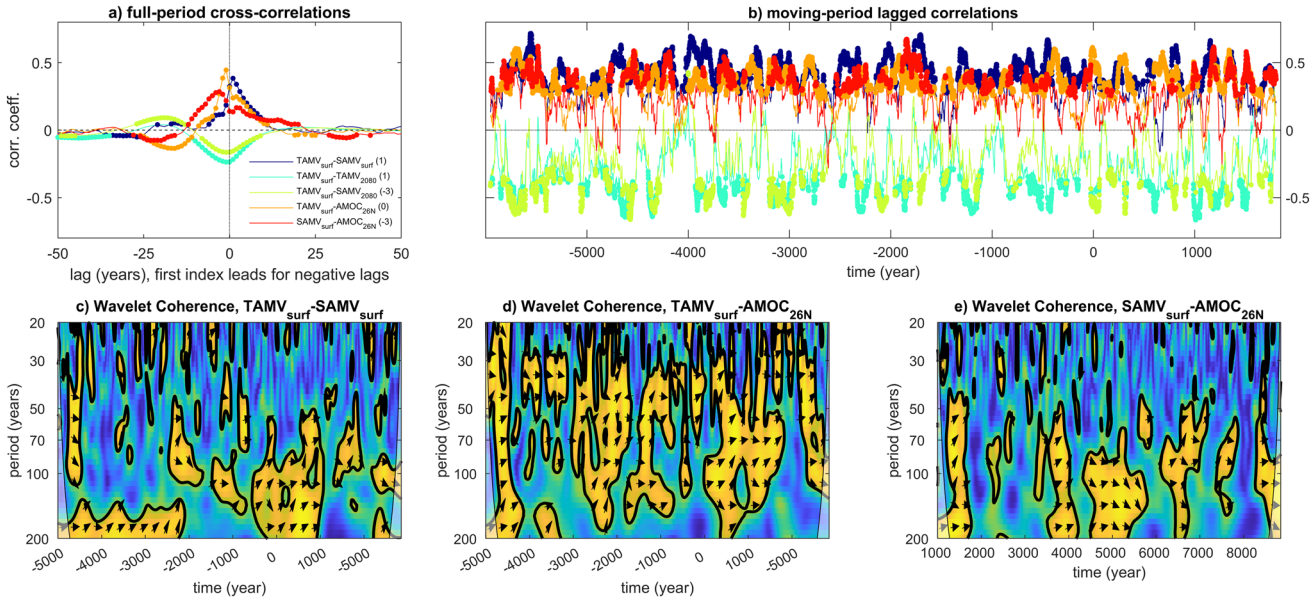

Fig. 7 Correlation and wavelet coherence across indices describing North Atlantic oceanic variability in Holo_GHG-ORB. **a** Full-period cross-correlations between annual paired indices; **b** Moving-window correlations, with window set to 91 years and for lags as reported in parentheses in the legend. Dots mark correlations significant at 95% confidence accounting for serial correlation in the indices. **c**–**e** Wavelet coherence spectra between paired annual indices. Representation as in Figs. 5 and 6

17 and 47 years for the cold-to-warm transition, as it refers to maximum and minimum TAMV$_{surf}$ anomalies within each event (see methods). The warm-to-cold transition is always associated with a broad and significant weakening of the overturning circulation, with a pattern that superposes well over the climatological correlation pattern between the meridional overturning streamfunction and TAMV$_{surf}$ (black contour in Fig. 8), despite peak negative values are located around 30° N, slightly north of the maximum of the climatological correlation pattern. This confirms that the oceanic evolution during the transition largely follows typical dynamics, i.e., dynamics that operate also outside periods of strong AMV fluctuations. The strengthening of the meridional overturning circulation during the cold-to-warm transition tends to mirror the weakening pattern during the preceding warm-to-cold transition. There is coherence in the amplitude and significance of anomalies across the events in the tropics and the midlatitudes, whereas warming anomalies are less coherent among the events at higher latitudes. The wavelet coherence spectra demonstrate that multidecadal AMOC variations lead the AMV. Otherwise, if surface dynamics were considered as a source for the AMOC changes during the events of strong AMV fluctuations, weakening of the thermohaline circulation under surface cooling could only be explained by a dominant effect of the surface freshening associated with the events. A separation of surface density anomalies in their temperature and salinity contributions indicates that the former largely dominate the latter (salinity only explains 20–25% of density changes), even in regions where large salinity anomalies occur during strong AMV fluctuations, due to strong temperature-driven density changes there (see supplementary Figure S1).

3.3 Spatial patterns of temperature and salinity anomalies during strong AMV events

This section describes the variability in the spatial patterns of thermohaline anomalies during events of strong AMV fluctuations in the form of temperature and salinity anomalies in the warm-to-cold and cold-to-warm transitions from the ensemble mean and the individual events S1, S3 and S8. Figure 9 shows the cooling and warming patterns of SST and SSS, focusing on the largest anomalies and hiding anomalies that contribute to the AMV signal but are not statistically significant.

Ensemble-mean SST anomalies (Fig. 9 top left panels) superpose well on the AMV basin-wide comma-shaped regression pattern (compare with Fig. 2d), yielding spatial correlations of 0.87 and 0.89 for the warm-to-cold and the cold-to-warm transition, respectively. Strong anomalies with coherent sign across ensemble members are found in the mid-latitude central North Atlantic and along the Canary current, and less coherent anomalies occur over the subpolar gyre region, especially in the cold-to-warm transition, and the western tropical and mid-latitude North Atlantic along and around the path of the Gulf Stream. As expected, ensemble-mean SSS anomalies (Fig. 9 top right panels) also superpose well on the climatological regression pattern onto

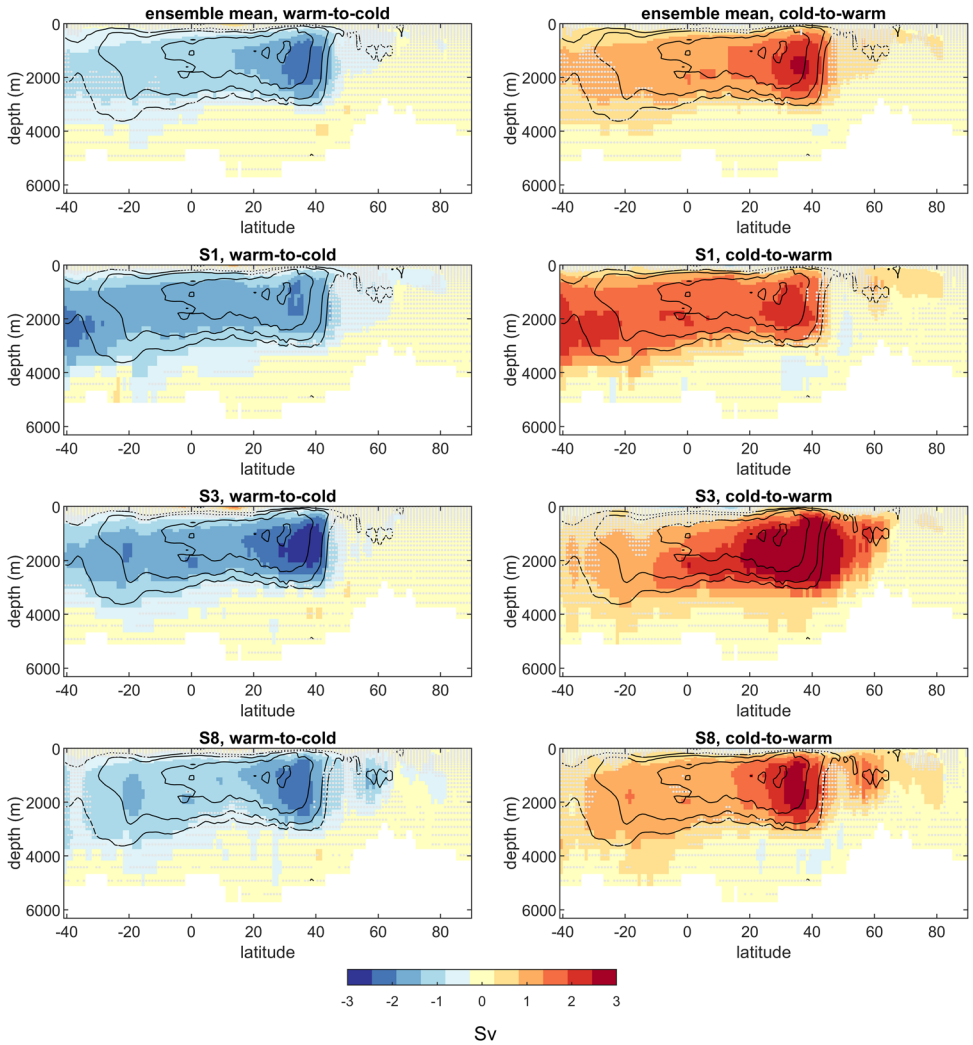

Fig. 8 Simulated anomalies of the meridional overturning streamfunction calculated for the warm-to-cold and the following cold-to-warm transitions of the simulated strong AMV fluctuations. Top: ensemble mean of twelve events; bottom: three selected events. Differences are between time means over 17-year periods around peak warm and cold AMV anomalies. Dots indicate where the differences are statistically not significant. For the ensemble, this means that the 10–90 percentile range of ensemble values encompasses the value of zero; for individual events, this means that local anomalies exceed the 10–90 percentile range obtained from the 17-year running-mean time series. The contour lines illustrate the correlation coefficients at r = 0.4, 0.5, 0.6 and 0.7 between the meridional overturning streamfunction and the $TAMV_{surf}$ time series, smoothed with a 17-year running mean

the AMV, yielding a spatial correlation of 0.91 for both the warm-to-cold and the cold-to-warm transitions. Coherent anomalies are largely confined in the mid-latitude eastern North Atlantic and, again, a remarkable symmetry between warm-to-cold and following cold-to-warm transitions. There is overall a broad overlap in sign between temperature and salinity anomalies, so that warming is associated with salinification and cooling with freshening.

Anomalies for S1, S3 and S8 (Fig. 9 mid and bottom panels, see supplementary Fig. S3 for all events) illustrate how the simulations represent the different shades of AMV anomalies detected in observations (Fig. 1c–f). For the warm-to-cold transition, spatial correlations between simulated and observed events range between −0.42 and 0.18 for E1, and between 0.09 and 0.43 for E2; for the cold-to-warm transition these values change to − 0.19 and 0.25 for E1, and 0.01 and 0.47 for E2 (see also Supplementary Figure S4). Spatial correlations are therefore generally low between simulated and observed patterns but also between patterns of different observed events. Both warm-to-cold and cold-to-warm transitions in different simulated events only partly overlap regarding the regions where significant SST and especially SSS anomalies occur. For instance, for the SST anomalies in the initial warm-to-cold transition, the subpolar North Atlantic is excluded in S1 whereas it is largely involved in S3 and S8. In the latter events, SST anomalies occur either around the core of the subpolar gyre (S3) or at its southeastern edge (S8). For SSS, the extent of non-significant regions in all individual events and in the ensemble-mean anomalous patterns implies that homogenous signs of anomalies over the basin do not generally occur. This is evident in S3, where a north–south dipole with significant anomalies of opposite sign in the subtropical and tropical eastern North Atlantic occur. Finally, symmetry between cooling and following warming patterns is not necessary, as shown by S1 for SST in the North and Greenland-Iceland-Norwegian Seas and for SSS in the tropical and midlatitude North Atlantic. Overall, despite the limited number of simulated events of strong AMV, the diversity of simulated surface patterns seems to be consistent with the diversity of patterns suggested by the

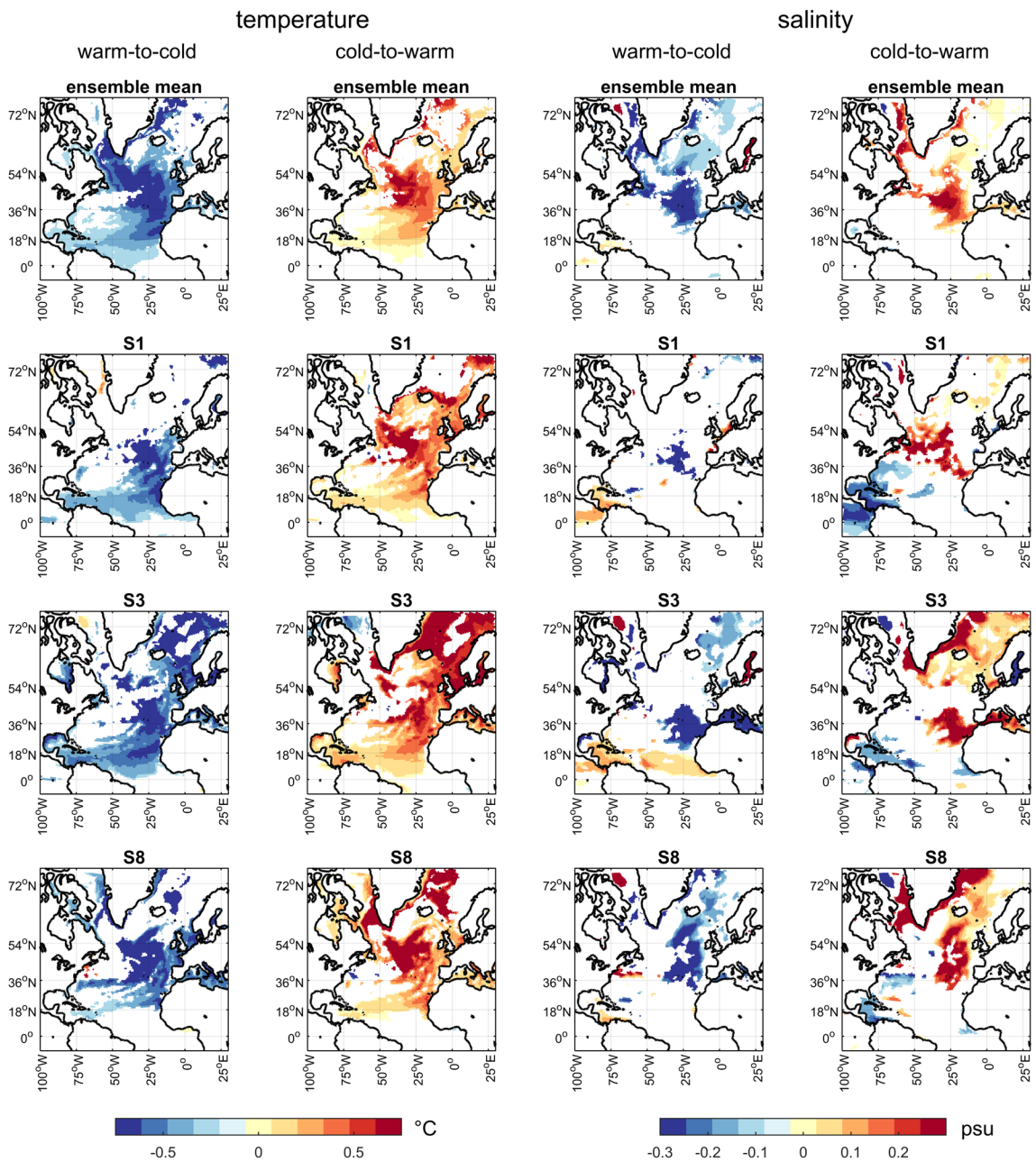

Fig. 9 Simulated SST (left panels) and SSS (right panels) anomalies calculated for the warm-to-cold and the following cold-to-warm transitions of the simulated strong AMV fluctuations. Top: ensemble mean of twelve events; bottom: three selected events. Differences are between time means over 17-year periods around peak warm and cold AMV anomalies. Only local anomalies that exceed the 25–75 percentile range obtained from the 17-year running-mean time series outside the period of strong AMV fluctuations are shown

observations concerning both position and sign of the significant anomalies.

It is more difficult to extract common features from temperature and salinity anomalies in the deep ocean. The ensemble-mean anomalies (Fig. 10, top panels) identify consistent (25–75 percentile range) changes among events associated with same-sign temperature and salinity anomalies and substantial symmetry in the warm-to-cold and following cold-to-warm transitions in the Irminger and Labrador Seas and, with anomalies of opposite sign, along the Gulf Stream. Only ensemble-mean anomalies in the southern part of the Irminger and eastern Labrador Sea are significant if a more restrictive range for significance (10–90 percentile range) is used. Anomalies are more extensive in individual events than in the ensemble mean,

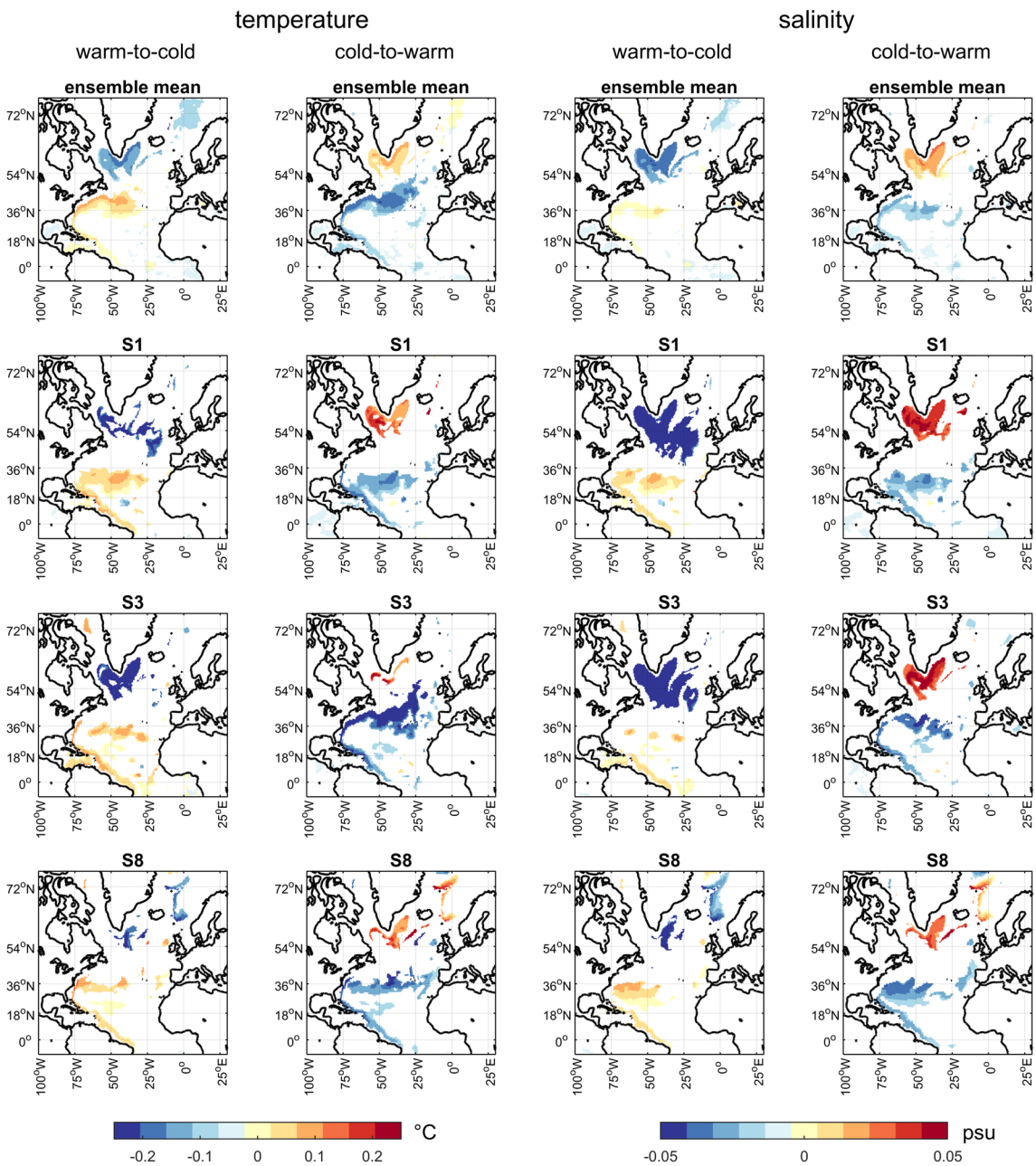

Fig. 10 Simulated deep ocean (2080 m depth) temperature and salinity anomalies calculated for the warm-to-cold and the following cold-to-warm transitions of the simulated strong AMV fluctuations. Representation as in Fig. 9. On top panels, grid points are shown where the 25–75 percentile range of ensemble members spans the value of zero, i.e., where the ensemble members disagree on the sign of the anomaly

confirming that the AMV pattern is less robust in the deep ocean (Fig. 10, mid and bottom panels).

Most events display a dipolar structure in deep thermohaline anomalies, with a clear asymmetry between the subpolar gyre region and the subtropics as shown by S1, S3 and S8 (see supplementary Figs. S5 and S6 for all events). The significant deep warm anomaly identified in Fig. 4a around and below 1000 m depth is hardly associable to a specific region of the basin despite most events featuring deep warming in the subtropical and/or mid-latitude region during the warm-to-cold transition. The existence of a dipolar structure in the deep layers is confirmed by significant coherence at inter-decadal scales between wavelet spectra of $TAMV_{surf}$ and of average seawater temperature in the deep ocean layer in the subpolar gyre (anti-phase) and Gulf Stream regions (in-phase) (see supplementary Figure S7). Also, there is again a

general symmetry between warm-to-cold and cold-to-warm anomalies, although this is reduced compared to surface conditions, as for instance seen in S1 and S3. Overall, the results point to a recurrent basin-scale dipolar pattern rather than to coherent changes in the thermohaline properties at depth, and to substantial variability in the cooling/freshening and warming/salinification patterns at depth during individual events of strong AMV variability.

The different shades of anomalous surface patterns of temperature and salinity simulated across different AMV events reflect differences in the ocean circulation forced by atmosphere–ocean coupled processes including wind forcing and surface heat fluxes and, especially at the mid latitudes, by variations in the ocean stratification. The spatial pattern of ensemble-mean anomalies in the barotropic mass streamfunction highlight the path of western boundary currents from the equator to the mid-latitudes, but there is lack of a coherent basin-scale pattern (Fig. 11, top panels). Patterns of individual events (Fig. 11, mid and bottom panels, and supplementary Fig. S8) demonstrate how the extent of significant wind-driven circulation anomalies can vary (compare for instance the warm-to-cold transitions in S1 and S3) and how the sign of the anomalies can be opposite in different events (compare S3 with S8 in the mid-latitudes during the cold-to-warm transition). Individual events also can lack symmetry between the warm-to-cold and following cold-to-warm transition (e.g., S1). Possibly, a non-significant yet recurrent feature is a north–south dipole in the midlatitudes along the Gulf Stream in the cold-to-warm transition, that resembles the inter-gyre gyre pattern. The wavelet coherence spectrum between $TAMV_{surf}$ and the subpolar gyre strength for piControl confirms lack of a robust connection at time scales relevant for the AMV (Fig. 6h). The only significant connection found in the wavelet coherence spectrum is an out-of-phase covariance at interdecadal and multidecadal timescales around years 3400–3600, where changes in the subpolar gyre lags AMV changes by several years. Such a potential gyre response to the AMV and its associated redistribution of ocean heat and salt may contribute to explain the weaker $TAMV_{surf}$-AMOC connection on multidecadal time scales observed during this time.

3.4 Impact of solar and volcanic forcings

Connections between surface and deep thermohaline variability and oceanic circulation are largely disrupted under transient conditions including solar and volcanic forcing (Fig. 12). In Holo_volc there is weak persistence of significant lagged $TAMV_{surf}$-$SAMV_{surf}$ correlations, similar to correlations obtained from piControl, but periods of significant correlation between $TAMV_{surf}$ and $TAMV_{2080}$, $SAMV_{2080}$ and AMOC become much more sporadic (Fig. 12b). The AMV_{surf}-AMOC wavelet coherence spectrum demonstrates

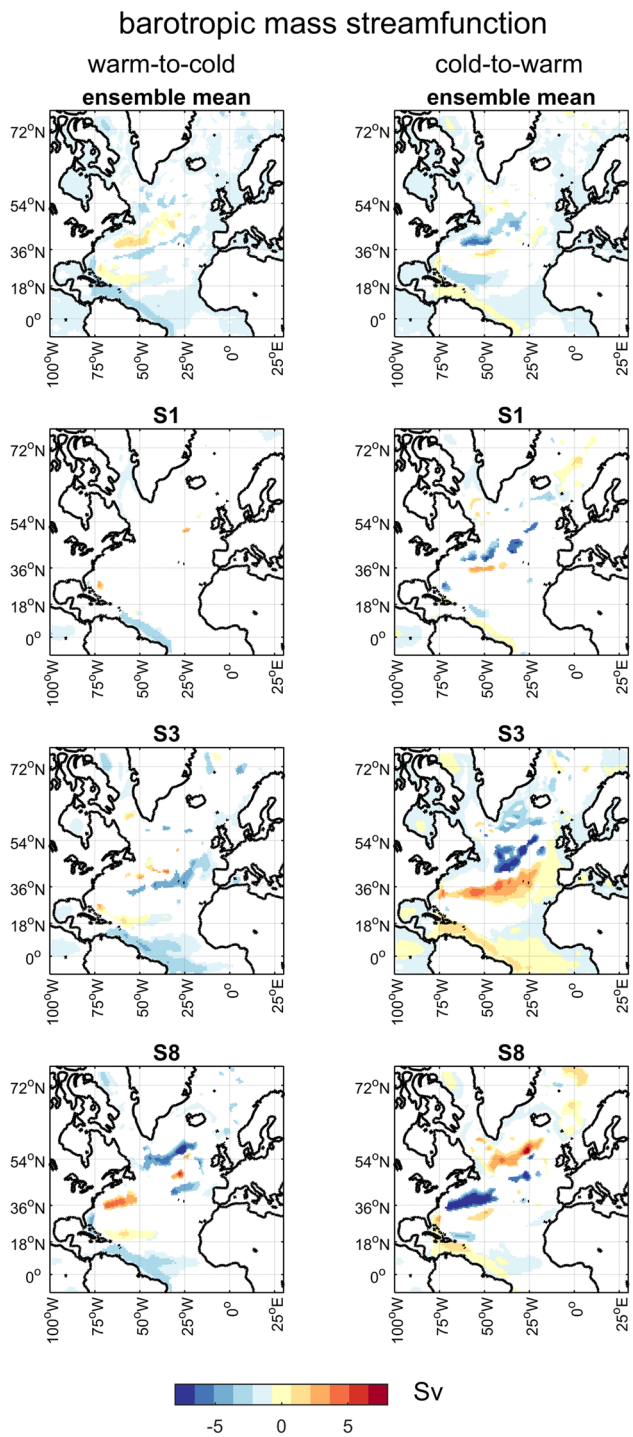

Fig. 11 Simulated anomalies of the ocean barotropic mass streamfunction calculated for the warm-to-cold and the following cold-to-warm transitions of the simulated strong AMV fluctuations. Representation as in Fig. 9. On top panels, grid points are shown where the 25–75 percentile range of ensemble members spans the value of zero, i.e., where the ensemble members disagree on the sign of the anomaly

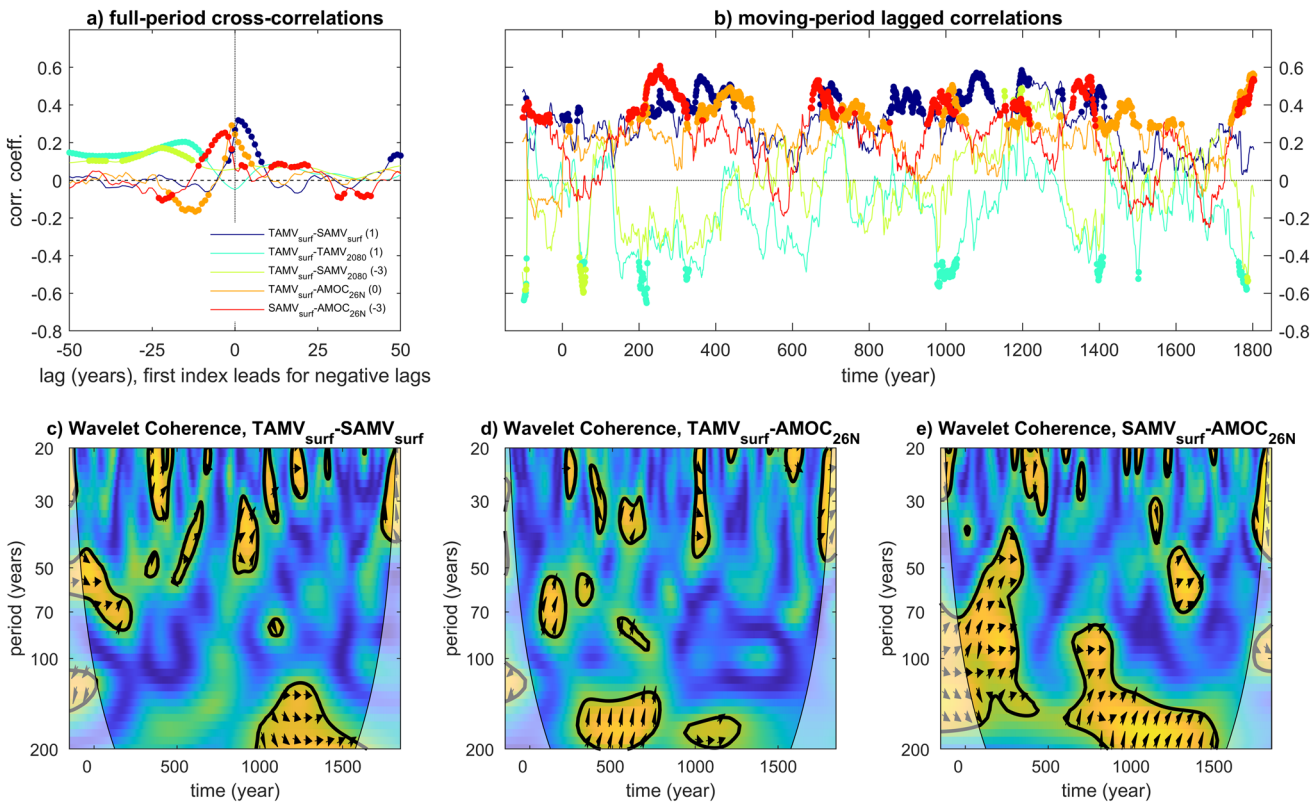

Fig. 12 Correlation and wavelet coherence across indices describing North Atlantic ocean variability in a transient paleoclimate simulation with MPI-ESM-LR covering the last 2000 years of the preindustrial period of the Common Era (from year − 150 to 1850 CE) including all forcings. **a** Full-period cross-correlations between annual paired indices; **b** Moving-window correlations, with window set to 91 years and for lags as reported in parentheses in the legend. Dots mark correlations significant at 95% confidence accounting for serial correlation in the indices. **c–e** Wavelet coherence spectra between paired annual indices. Representation as in Fig. 7

that variability of both variables is only sporadically connected at interannual to multidecadal time scales under the effects of volcanic forcing (Fig. 12d), where it is largely persistent throughout the simulation under unperturbed conditions and transient conditions excluding volcanic forcing (Figs. 6 and 7d). Accordingly, basin-scale surface warming and cooling phases of the North Atlantic become more decoupled from the thermohaline circulation under volcanic forcing. Alternatively, volcanic forcing triggers multiple mechanisms linking TAMV$_{surf}$ and AMOC that differ from intrinsic dynamics and yield an overall weak connection between both variables. This can be understood, for instance, by contrasting the intrinsic positive correlation between TAMV$_{surf}$ and AMOC with their negative correlation due to post-eruption surface cooling contributing to post-eruption AMOC strengthening.

Four events of strong AMV fluctuations similar to observed historical AMV fluctuations are extracted from Holo_volc, starting around years 35, 114, 490 and 1067. None of these events occur in concomitance with a major volcanic eruption. However, the differences in correlation and wavelet coherence spectra among key variables during these events (Fig. 12b–e) suggest that they are associated with different dynamics. North Atlantic SST anomalies following sixteen major volcanic eruptions from the evolv2k volcanic history that was used to generate volcanic forcing in Holo_volc (see methods), indicate that volcanic forcing can significantly imprint on the temporal evolution of indices and anomalous spatial patterns associated with the AMV (Fig. 13). Post-eruption surface cooling in the North Atlantic can last for up to a decade following major eruptions (Fig. 13a) with extensive cold anomalies over the North Atlantic in the ensemble mean but not over the tropical western and the near-equatorial regions, and with weak anomalies over the mid-latitude and subpolar North Atlantic where the AMV regression pattern on SSTs yields the strongest signal (compare Fig. 13c with Fig. 2d).

Due to pacing between volcanic eruptions, forced fluctuations emerge on timescales compatible with the intrinsic AMV dynamics (see, for instance, the three times the large cooling after the 1257 Samalas eruption appears in the ensemble plot). After major eruptions, there is no robust basin-scale anomalous SSS signal (Fig. 13b), which contrasts with dynamics found under unperturbed conditions. Accordingly,

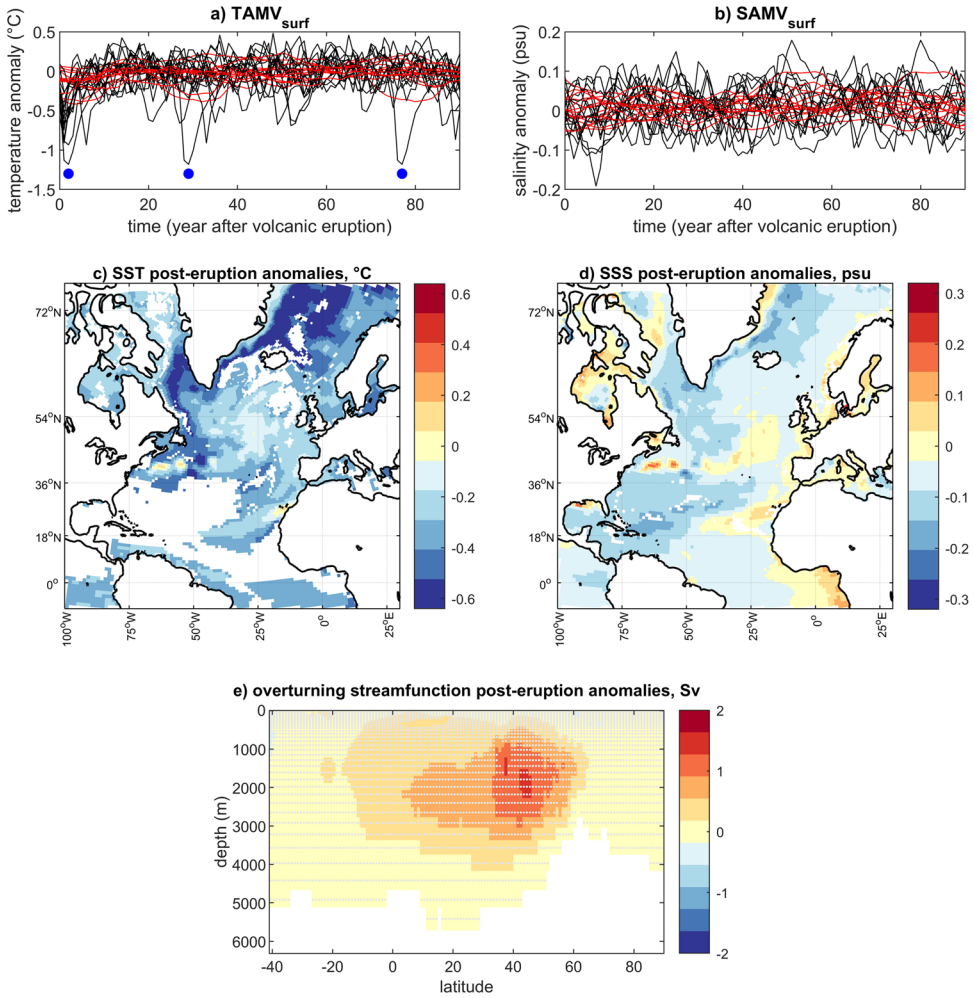

Fig. 13 Simulated AMV anomalies following major volcanic eruptions. **a**, **b** temporal evolution of $TAMV_{surf}$ (**a**) and $SAMV_{surf}$ (**b**) indices (annual: black; smoothed, 17-year running mean: red); **c**, **d** ensemble-mean anomalous spatial patterns of SST (**c**) and SSS (**d**) for the first 10 years following the eruptions; **e** ensemble-mean anomaly of the Atlantic meridional overturning streamfunction for the first 10 years following the eruptions. In **a**, **b** anomalies the same eruption can be plotted more than once if it occurred in the aftermath of preceding events within the 90 year period considered here (the case of 1257 Samalas is highlighted by blue dots in **a**). Significance is shown following ensemble-mean analysis in Figs. 8e and 9c, d

the ensemble-mean post-eruption anomalous spatial pattern of surface salinity is complex and consists of intertwined positive and negative anomalies that do not overlap on the regression pattern of AMV on SSS (compare Fig. 13d and Fig. 2e). In contrast to the AMOC weakening in correspondence to the cold AMV phase obtained for events of strong intrinsic AMV fluctuations, a tendency toward post-eruption AMOC strengthening is seen in post-eruption years, as a response to the volcanically forced surface cooling (Fig. 13e). The AMOC strengthening is, however, significant only in a limited region (around 35° N latitude and 1000 m of depth) and not at latitudes and depths where the anomalies are strongest (around 45° N latitude and 2000 m of depth), meaning that the volcanically forced AMOC response has a low signal-to-noise ratio in MPI-ESM-LR.

4 Discussion

Strong multidecadal fluctuations in spatially averaged North Atlantic SST, with an amplitude of around 0.3 °C, arise intermittently only due to intrinsic variability in an unperturbed coupled climate model simulation and in a Holocene transient simulation including only slow-varying forcing. These fluctuations are comparable in amplitude and duration with historical AMV features observed at the surface, despite the latter include the potential effects of external forcing agents not included in our simulations. Differently from the observed AMV pattern, which highlights the western mid-latitude North Atlantic, the simulated AMV pattern exhibits large values in the central

mid-latitude North Atlantic, where the CMIP5 version of MPI-ESM-LR shows a cold surface bias (Jungclaus et al. 2013). The simulated AMV events share common characteristics. For instance, basin-scale SST variability is generally associated with same sign fluctuations in SSS and there is a tendency for basin-average deep ocean temperature and salinity anomalies to be in anti-phase with corresponding surface signals during such events, this spatially integrated behavior masking an even clearer meridional dipolar pattern between thermohaline anomalies in the deep subpolar and subtropical portions of the North Atlantic.

The anomalous SST patterns for cooling and warming AMV phases highlight the North Atlantic subpolar gyre region where the strongest heat convergence associated with the meridional ocean heat transport occurs (e.g., Delworth et al. 2016; Omrani et al. 2022). Furthermore, SST anomalies consistent with a dominant effect of anomalous poleward ocean heat transport are found in polar regions, where they reflect sea-ice changes, and in the tropical North Atlantic, where heat divergence (i.e., cooling effect) is strongest and SST warming, in case of a positive AMV phase, is generally maintained by stratosphere/troposphere-coupled dynamics (Omrani et al. 2022). Therefore, all indications point toward a generally strong and roughly co-phased connection between AMV-like fluctuations in North Atlantic SST and changes in the strength of the ocean thermohaline circulation, more specifically the AMOC. Our study therefore supports the important role of the AMOC as a pacemaker of the AMV (e.g., Zhang 2017; Oelsmann et al. 2020; Omrani et al. 2022).

Dynamical interpretation of the tight AMOC–AMV connection can be built on Oelsmann et al. (2020), who used a set of idealized experiments with MPI-ESM to separate the contributions of atmospheric and ocean dynamics for the AMV. Accordingly, for the warm-to-cold transitions that constitute the first part of the strong AMV events, weakening of the AMOC leads to ocean heat divergence, hence heat dispersion, in the subpolar North Atlantic; then, coupling with atmosphere favors the spreading of heat anomalies and yields the basin-wide surface cooling pattern associated with the AMV. The opposite occurs during the following cold-to-warm transition.

Omrani et al. (2022) recently used last-millennium simulations with an earlier version of MPI-ESM to demonstrate that multidecadal northern-hemisphere winter variability can be understood within a damped coupled stratosphere/troposphere/ocean-oscillation framework. In their interpretation, consistent with Oelsmann et al. (2020), an AMOC strengthening initiated by large-scale atmospheric anomalies drives an AMV-like warming through strengthened poleward oceanic heat transport. The damped character of the AMV illustrated by Omrani et al. (2022), with the damping time scales set by ocean dynamics (Sun et al. 2015), can explain the intermittent nature of the AMV. Whereas our wavelet analysis provides consistent results with Oelsmann et al. (2020) and Omrani et al. (2022) concerning the phasing between AMV and AMOC on multidecadal timescales, cross-correlations suggest a tighter AMV–AMOC co-variability. This may be related to interannual variability embedded in the AMV index, which might contain an imprint on SST of atmospheric circulation anomalies, or to the choices in the index definition, e.g., for the AMOC its value at 26.5° N (the largest anomalies during strong AMV fluctuations appear north of this latitude).

Other models may yield different AMOC mechanisms relevant for the AMV. Among them, potentially relevant is large-scale baroclinic instability (e.g., Arzel et al. 2018; Gastineau et al. 2018). The wavelet coherence showing phase lags in quadrature between surface and deep temperature anomalies in the Gulf Stream region, where SST variability is strongest, indicates that this mechanism may be intermittently active in MPI-ESM-LR on bidecadal time scales, but not on the multidecadal time scales relevant for the AMV (supplementary Figure S9). Further analyses may determine if the identification of the mechanism is sensitive to the choice of the region where the analysis is conducted.

The role of salinity anomalies as co-driver of the AMV–AMOC mechanism deserves further investigation. Based on our analysis, SSS contributes only to up to 25% of surface density changes during strong AMV fluctuations. The SSS patterns highlight the eastern mid-latitude North Atlantic, which relates with wind-driven changes in the path of the Gulf Stream, and the internal portion of the Labrador Sea, which may relate to sea-ice dynamics as discussed above (see Omrani et al. 2022). The CMIP5 multi-model study by Menary et al. (2015) revealed a dependency of the mechanisms of simulated decadal variability in the North Atlantic subpolar gyre region on the models' mean state, especially salinity-driven density biases in the Labrador Sea. The CMIP5 version of MPI-ESM-LR shows a warm and salty surface bias in the Labrador Sea (Jungclaus et al. 2013), which according to Menary et al. (2015) corresponds to a temperature-controlled mechanism of North Atlantic subpolar gyre decadal variability. This bias dependency may be relevant also for the AMV and, if confirmed, would render the role of salinity anomalies more relevant than envisaged here.

The North Atlantic Oscillation or NAO is often invoked as a source for simulated AMOC variability (e.g., Delworth and Zeng 2016; Oelsmann et al. 2020). The NAO may also play a role in the establishment of warm AMV phases through acting on the tropical branch of the AMV, for instance through maintaining warm tropical SST anomalies via the wind-evaporation-SST feedback (Omrani et al. 2022). However, the link between the NAO and AMV may

be timescale dependent, and the damped oscillation identified by Omrani et al. (2022) extracts coherent multidecadal fluctuations across stratosphere, troposphere and the Atlantic with a timescale around 50 years, which is shorter than the observed AMV timescale used in this study. Also, the role of the NAO may depend on the model resolution and be weaker in coarser models or model versions (Lai et al. 2022). Our analysis indicates a significant yet small negative full-period correlation where the NAO leads AMOC and AMV by a few years (Fig. 5a), but not all identified events of strong AMV feature a significant NAO imprint (see for instance the case of event S1). This suggests that other large-scale modes of atmospheric variability imprinting on oceanic circulation in the North Atlantic subpolar gyre region may be relevant to trigger strong AMV fluctuations, for instance modes linked with changes in the frequency and intensity of atmospheric blocking (e.g., Moreno-Chamarro et al. 2017a).

Beyond the common traits discussed above, the simulated spatial patterns and the vertical propagation of anomalous temperature and salinity signals can differ between different periods characterized by strong AMV fluctuations, like the diversity of patterns obtained from observations. As shown for a multi-millennial unperturbed simulation with a previous version of MPI-ESM (Zanchettin et al. 2016a), the specificities of AMV anomalies reflect temporal variations of the covariance pattern of North Atlantic SSTs. Accordingly, the wind-driven circulation may contribute to the specificities of strong AMV events as anomalies in the simulated barotropic streamfunction often include significant changes along the Caribbean current and the Gulf Stream current path during strong AMV fluctuations. However, the anomalies differ in sign in different events and there is little symmetry between patterns in the warm-to-cold and following cold-to-warm AMV transitions. The inter-gyre gyre pattern found in some of the simulated barotropic streamfunction anomalies may be an expression of the coupling between AMOC and the North Atlantic subpolar gyre (Yaeger 2015). However, there is no robust connection between intrinsic variability of AMV and of the strength of the North Atlantic subpolar gyre in our simulations.

The simulated intrinsic characteristics of AMV are modified by external perturbations acting on the AMV typical timescales. This is seen by the substantial changes in the connections between seawater temperature, salinity and the AMOC found under unperturbed or Holocene transient conditions with only slow-varying external forcing and under Holocene transient conditions with active solar and volcanic forcing. For instance, the tight connection between SST and the overturning circulation is weakened when volcanic forcing is active, while SSS shows a more persistent connection with SST variations under slow-varying transient orbital and greenhouse gas forcing. The weakening of the AMOC–AMV connection can be explained by a tendency (statistically not significant in our analysis) toward temporary AMOC strengthening forced by surface cooling in post-eruption years. In general, our findings agree with multi-model analyses where external forcing is found to interfere with the typical unforced relationship between the AMOC and North Atlantic SST (e.g., Otterå et al. 2010; Tandon and Kushner 2015). Further, the pacing of volcanic eruptions may lead to externally forced AMV fluctuations on timescales compatible with those characteristics of internal dynamics, as noted by previous studies (e.g., Zanchettin et al. 2010; Mann et al. 2021).

The different connections between surface and deep thermohaline properties and thermohaline circulation under different imposed boundary forcing can help characterize AMV-like fluctuations in paleoclimate simulations (e.g., Mann et al. 2021; Fang et al. 2021) and better evaluate proxy-based reconstructions. Overall, beyond the specificities of the single model used here, fingerprinting and attribution of AMV-like events seems to be facilitated by a three-dimensional spatial characterization of associated thermohaline anomalies. This could be also helpful for the historical AMV as the consideration of anthropogenic forcing and mean-state changes does not affect the general validity of our approach: characterization and analysis of interior ocean thermohaline anomalies since the mid-nineteenth century could contribute to the debate on the nature—externally forced rather than predominantly intrinsic—of the historical AMV.

5 Conclusions

The Atlantic Multidecadal Variability (AMV) was characterized in three multi-millennial climate simulations with MPI-ESM-LR including an unperturbed control simulation, a Holocene transient simulation with only slow-varying greenhouse gas and orbital forcing, and a full-forcing Holocene transient simulation. A tight AMV–AMOC connection dominates variability in the first two simulations, with AMOC weakening corresponding to AMV cooling and vice versa. Therefore, in MPI-ESM-LR, the AMV can emerge as an expression of intrinsic climate dynamics with a major role for the ocean. Accordingly, anomalous patterns emerge in temperature and salinity at depth around major events of AMV fluctuations. The AMV–AMOC connection is disrupted in the third simulation, arguably due to volcanic surface cooling interfering with intrinsic coupled ocean–atmosphere dynamics. Post-eruption years are characterized by surface cooling and associated tendency toward AMOC strengthening, which contrasts with the unperturbed AMOC–AMV relation. Twelve events of strong AMV fluctuations were extracted from the unperturbed simulation and the Holocene simulation

with slow-varying forcing, which superposed well on observed AMV fluctuations during the historical period. If anthropogenic forcing disrupts the AMOC–AMV relation as fast natural forcing does, the obtained comparability of AMV surface characteristics in historical observations and unperturbed/slowly perturbed simulations indicates that robust attribution of the historical AMV is possible only by accounting for subsurface anomalies and by assessing the AMOC–AMV relation.

Individual events of strong intrinsic AMV variability share significant same-sign sea-surface temperature and salinity anomalies in the mid-latitude central and eastern North Atlantic, while anomalies are less coherent across events over the North Atlantic subpolar region and the tropics. At depth, significant thermohaline anomalies of opposite sign with respect to the surface are robustly found in the subpolar gyre region; less coherently across individual events, thermohaline anomalies of same sign with respect to the surface are robustly found in the midlatitudes. A dipolar meridional thermohaline pattern in the ocean interior is thus recurrent in intrinsic strong AMV fluctuations simulated by MPI-ESM-LR. Individual events also differ in the timings and duration of their warm-to-cold and following cold-to-warm transitions. A multi-model verification of the single model results obtained in this study may serve to better understand the different shades of this multidecadal mode of climate variability.

Supplementary Information The online version contains supplementary material available at https://doi.org/10.1007/s00382-023-06679-w.

Acknowledgements Simulations were performed at the Deutsches Klimarechenzentrum (DKRZ). Maps are plotted with the m_map package (Pawlowicz 2000) for MATLAB software, using the GSHHG dataset for coastlines (Wessel and Smith 1996). Map colors based on http://www.ColorBrewer.org, by Cynthia A. Brewer, Penn State. We thank two anonymous reviewers for their helpful comments.

Authors contributions DZ conceived the study, performed the analyses, wrote the initial manuscript and revised it. SWF computed the indices. All authors contributed to discussion and finalization of the manuscript.

Funding This work was supported by the German Federal Ministry of Education and Research (BMBF) within the research programme "ROMIC-II, ISOVIC" (FKZ: 01LG1909B, SWF) and the Deutsche Forschungsgemeinschaft Research Unit VolImpact (FOR2820, Grant no. 398006378, CT) within the project VolClim. N-EO is supported by the Bjerknes Climate Prediction Unit funded by the Trond Mohn Foundation (Grant BFS2018TMT01), the RCN funded ROADMAP project (Grant 316618) under a joint JPI Climate and JPI Ocean call and the Impetus4Change funded by European Union's Horizon Europe research and innovation program (Grant 101081555).

Data availability Primary data and scripts used in the analysis and other supplementary information that may be useful in reproducing this work will be archived by the Max Planck Institute for Meteorology upon final publication.

Declarations

Conflict of interest The authors have no relevant financial or non-financial interests to disclose.

Ethics approval and consent to participate Not applicable.

Consent for publication Not applicable.

References

Arzel O, Huck T, de Verdière AC (2018) The internal generation of the atlantic ocean interdecadal variability. J Clim 31:6411–6432

Bader J, Jungclaus J, Krivova N, Lorenz S, Maycock A, Raddatz T, Schmidt H, Toohey M, Wu C-J, Claussen M (2020) Global temperature modes shed light on the Holocene temperature conundrum. Nat Commun 11:4726. https://doi.org/10.1038/s41467-020-18478-6

Bellomo K, Murphy LN, Cane MA, Clement AC, Polvani LM (2018) Historical forcings as main drivers of the Atlantic multidecadal variability in the CESM large ensemble. Clim Dyn 50(9–10):3687–3698. https://doi.org/10.1007/s00382-017-3834-3

Bellucci A, Mariotti A, Gualdi S (2017) The role of forcings in the twentieth-century North Atlantic multidecadal variability: the 1940–75 North Atlantic cooling case study. J Clim 30(18):7317–7337. https://doi.org/10.1175/JCLI-D-16-0301.1

Birkel SD, Mayewski PA, Maasch KA, Kurbatov AV, Lyon B (2018) Evidence for a volcanic underpinning of the Atlantic multidecadal oscillation. NPJ Clim Atmos Sci 1(1):1–7

Boer GJ, Smith DM, Cassou C, Doblas-Reyes F, Danabasoglu G, Kirtman B, Kushnir Y, Kimoto M, Meehl GA, Msadek R, Mueller WA, Taylor KE, Zwiers F, Rixen M, Ruprich-Robert Y, Eade R (2016) The Decadal Climate Prediction Project (DCPP) contribution to CMIP6. Geosci Model Dev 9:3751–3777. https://doi.org/10.5194/gmd-9-3751-2016

Booth BBB, Dunstone NJ, Halloran PR, Andrews T, Bellouin N (2012) Aerosols implicated as a prime driver of twentieth-century North Atlantic climate variability. Nature. https://doi.org/10.1038/nature10946

Clement A, Bellomo K, Murphy LN, Cane MA, Mauritsen T, Rädel G, Stevens B (2015) The Atlantic Multidecadal Oscillation without a role for ocean circulation. Science 350(6258):320–324. https://doi.org/10.1126/science.aab3980

Clement A, Bellomo K, Murphy LN, Cane MA, Mauritsen T, Stevens B (2016) Response to comment on "The Atlantic Multidecadal Oscillation without a role for ocean circulation." Science 352(6293):1527. https://doi.org/10.1126/science.aaf2575

Dallmeyer A, Claussen M, Lorenz S, Sigl M, Toohey M, Herzshuh U (2021) Holocene vegetation transitions and their climatic drivers in MPI-ESM1.2. Clim past 17:2481–2513. https://doi.org/10.5194/cp-17-2481-2021

Dawdy DR, Matalas NC (1964) Statistical and probability analysis of hydrologic data, part III: Analysis of variance, covariance and time series. In: Chow VT (ed) Handbook of applied hydrology, a compendium of water-resources technology. McGraw-Hill Book Company, New York, p 8.68-8.90

Delworth TL, Mann ME (2000) Observed and simulated multidecadal variability in the Northern Hemisphere. Clim Dyn 16:661–676. https://doi.org/10.1007/s003820000075

Delworth TL, Zeng F (2016) The impact of the north Atlantic oscillation on climate through its influence on the Atlantic meridional

overturning circulation. J Clim 29:941–962. https://doi.org/10.1175/JCLI-D-15-0396.1

Delworth TL et al (2016) The North Atlantic Oscillation as a driver of rapid climate change in the Northern hemisphere. Nat Geosci 9:509

Dima M, Lohmann G (2007) A hemispheric mechanism for the Atlantic Multidecadal Oscillation. J Clim 20:2706–2719. https://doi.org/10.1175/JCLI4174.1

Enfield DB, Mestas-Nunez AM, Trimble PJ (2001) The Atlantic multidecadal oscillation and its relationship to rainfall and river flows in the continental U.S. Geophys Res Lett 28:2077–2080

Fang SW, Khodri M, Timmreck C, Zanchettin D, Jungclaus JH (2021) Disentangling internal and external contributions to Atlantic multidecadal variability over the past millennium. Geophys Res Lett 48(23):e2021GL095990

Frajka-Williams E, Beaulieu C, Duchez A (2017) Emerging negative Atlantic Multidecadal Oscillation index in spite of warm subtropics. Sci Rep 7:11224

Gastineau G, Mignot J, Arzel O, Huck T (2018) North Atlantic Ocean internal decadal variability: role of the mean state and ocean-atmosphere coupling. J Geophys Res Oceans 123:5949–5970

Giorgetta MA, Jungclaus J, Reick CH, Legutke S, Bader J, Böttinger M, Brovkin V, Crueger T, Esch M, Fieg K, Glushak K, Gayler V, Haak H, Hollweg H, Ilyina T, Kinne S, Kornblueh L, Matei D, Mauritsen T, Mikolajewicz U, Mueller W, Notz D, Pithan F, Raddatz T, Rast S, Redler R, Roeckner E, Schmidt H, Schnur R, Segschneider J, Six KD, Stockhause M, Timmreck C, Wegner J, Widmann H, Wieners K, Claussen M, Marotzke J, Stevens B (2013) Climate and carbon cycle changes from 1850 to 2100 in MPI-ESM simulations for the Coupled Model Intercomparison Project phase 5. J Adv Model Earth Syst 5:572–597

Gray ST, Graumlich LJ, Betancourt JL, Pederson GT (2004) A treering based reconstruction of the Atlantic multidecadal oscillation since 1567 AD. Geophys Res Lett 31:L12205

Grinsted A, Moore JC, Jevrejeva S (2004) Application of the cross wavelet transform and wavelet coherence to geophysical time series. Nonlinear Process Geophys 11:561–566

Hand R, Bader J, Matei D, Ghosh R, Jungclaus JH (2020) Changes of decadal SST variations in the subpolar North Atlantic under strong CO_2 forcing as an indicator for the ocean circulation's contribution to Atlantic Multidecadal Variability. J Clim 33:3213–3228

Hodson DLR et al (2022) Coupled climate response to Atlantic Multidecadal Variability in a multi-model multi-resolution ensemble. Clim Dyn 59:805–836

Ilyina T, Six KD, Segschneider J, Maier-Reimer E, Li H, Nunez-Riboni I (2013) Global ocean biogeochemistry model HAMOCC: model architecture and performance as component of the MPI-Earth system model in different CMIP5 experimental realizations. J Adv Model Earth Sys 5:287–315. https://doi.org/10.1029/2012MS000178

Jiang W, Gastineau G, Codron F (2021) Multicentennial variability driven by salinity exchanges between the Atlantic and the Arctic Ocean in a coupled climate model. J Adv Model Earth Syst 13:e2020M002366

Jungclaus JH, Haak H, Latif M, Mikolajewicz U (2005) Arctic–North Atlantic interactions and multidecadal variability of the meridional overturning circulation. J Clim 18:4013–4031. https://doi.org/10.1175/JCLI3462.1

Jungclaus JH, Fischer N, Haak H, Lohmann K, Marotzke J, Matei D, Mikolajewicz U, Notz D, von Storch JS (2013) Characteristics of the ocean simulations in the Max Planck Institute Ocean Model (MPIOM) the ocean component of the MPI-Earth system model. J Adv Model Earth Syst 5:422–446. https://doi.org/10.1002/jame.20023

Jungclaus JH, Lohmann K, Zanchettin D (2014) Enhanced 20th-century heat transfer to the Arctic simulated in the context of climate variations over the last millennium. Clim past 10:2201–2213. https://doi.org/10.5194/cp-10-2201-2014

Jungclaus JH et al (2017) The PMIP4 contribution to CMIP6—part 3: the last millennium, scientific objective and experimental design for the PMIP4 past1000 simulations. Geosci Model Dev 10:4005–4033. https://doi.org/10.5194/gmd-10-4005-2017

Klavans JM, Clement AC, Cane MA, Murphy LN (2022) The evolving role of external forcing in North Atlantic SST variability over the last millennium. J Clim 35:1–44

Knight JR (2009) The Atlantic multidecadal oscillation inferred from the forced climate response in coupled general circulation models. J Clim 22:1610–1625

Knight JR, Folland CK, Scaife AA (2006) Climate impacts of the Atlantic Multidecadal Oscillation. Geophys Res Lett 33:L17706. https://doi.org/10.1029/2006GL026242

Lai WKM, Robson JI, Wilcox LJ, Dunstone N (2022) Mechanisms of internal Atlantic Multidecadal variability in HadGEM3-GC3.1 at two different resolutions. J Clim 35:1365–1383

Li X, Holland DM, Gerber EP, Yoo C (2014) Impacts of the north and tropical Atlantic Ocean on the Antarctic Peninsula and sea ice. Nature 505:538–542

Li L, Lozier MS, Buckley MW (2020) An investigation of the ocean's role in Atlantic multidecadal variability. J Clim 33(8):3019–3035

Maher N, Milinski S, Suarez-Gutierrez L, Botzet M, Dobrynin M, Kornblueh L et al (2019) The Max Planck Institute Grand Ensemble: Enabling the exploration of climate system variability. J Adv Model Earth Syst 11:2050–2069. https://doi.org/10.1029/2019MS001639

Mann ME, Steinman BA, Brouillette DJ, Miller SK (2021) Multidecadal climate oscillations during the past millennium driven by volcanic forcing. Science 371(6533):1014–1019

Marsland SJ, Haak H, Jungclaus JH, Latif M, Roeske F (2003) The Max Planck Institute global ocean/sea ice model with orthogonal curvilinear coordinates. Ocean Modell 5:91–127

Martín-Rey M, Rodríguez-Fonseca B, Polo I (2015) Atlantic opportunities for ENSO prediction. Geophys Res Lett 42:6802–6810. https://doi.org/10.1002/2015GL065062

Mauritsen T, Bader J, Becker T, Behrens J, Bittner M, Brokopf R, Brovkin V, Claussen M, Crueger T, Esch M, Fast I, Fiedler S et al (2019) Developments in the MPI-M Earth System Model version 1.2 (MPI-ESM1.2) and its response to increasing CO_2. J Adv Model Earth Sy 11:998–1038. https://doi.org/10.1029/2018MS001400

Meccia VL, Fuentes-Franco R, Davini P et al (2022) Internal multicentennial variability of the Atlantic Meridional Overturning Circulation simulated by EC-Earth3. Clim Dyn. https://doi.org/10.1007/s00382-022-06534-4

Medhaug I, Furevik T (2011) North Atlantic 20th century multidecadal variability in coupled climate models: sea surface temperature and ocean overturning circulation. Ocean Sci 7:389–404. https://doi.org/10.5194/os-7-389-2011

Meehl GA, Hu A, Castruccio F, England MH, Bates SC, Danabasoglu G, McGregor S, Arblaster JM, Xie S-P, Rosenbloom N (2021) Atlantic and Pacific tropics connected by mutually interactive decadal-timescale processes. Nat Geosci 14:36–42

Menary MB, Hodson DLR, Robson JI, Sutton RT, Wood RA, Hunt JA (2015) Exploring the impact of CMIP5 model biases on the simulation of North Atlantic decadal variability. Geophys Res Lett 42:5926–5934

Moore GWK, Halfar J, Majeed H, Adey W, Kronz A (2017) Amplification of the Atlantic Multidecadal Oscillation associated with the onset of the industrial-era warming. Sci Rep 7:40861

Moreno-Chamarro E, Zanchettin D, Lohmann K, Jungclaus JH (2015) Internally generated decadal cold events in the northern North Atlantic and their possible implications for the demise of the Norse settlements in Greenland. Geophys Res Lett 42(3):908–915. https://doi.org/10.1002/2014GL062741

Moreno-Chamarro E, Zanchettin D, Lohmann K, Luterbacher J, Jungclaus JH (2017a) Winter amplification of the European Little Ice Age cooling by the subpolar gyre. Sci Rep 7:9981. https://doi.org/10.1038/s41598-017-07969-0

Moreno-Chamarro E, Zanchettin D, Lohman K, Jungclaus JH (2017b) An abrupt weakening of the subpolar gyre as trigger of Little Ice Age-type episodes. Clim Dyn 48(3–4):727–744. https://doi.org/10.1007/s00382-016-3106-7

Murphy LN, Bellomo K, Cane M, Clement A (2017) The role of historical forcings in simulating the observed Atlantic multidecadal oscillation. Geophys Res Lett 44:2472–2480. https://doi.org/10.1002/2016GL071337

Oelsmann J, Borchert L, Hand R, Baehr J, Jungclaus JH (2020) Linking ocean forcing and atmospheric interactions to Atlantic multidecadal variability in MPI-ESM1.2. Geophys Res Lett 47:e2020GL087259. https://doi.org/10.1029/2020GL087259

Oldenburg D, Wills RC, Armour KC, Thompson L, Jackson LC (2021) Mechanisms of low-frequency variability in North Atlantic Ocean heat transport and AMOC. J Clim 34(12):4733–4755

Omrani N-E, Keenlyside N, Matthes K, Boljka L, Zanchettin D, Jungclaus JH, Lubis SW (2022) Coupled stratosphere-troposphere-Atlantic multidecadal oscillation and its importance for near-future climate projection. Npj Clim Atmos Sci 5:59. https://doi.org/10.1038/s41612-022-00275-1

Otterå OH, Bentsen M, Drange H, Suo L (2010) External forcing as a metronome for Atlantic multidecadal variability. Nat Geosci. https://doi.org/10.1038/NGEO995

Pawlowicz R (2000) M_Map: a mapping package for Matlab. University of British Columbia Earth and Ocean Sciences[Online]. http://www.eosubcca/rich/maphtml

Polyakov IV, Bhatt US, Simmons HL, Walsh D, Walsh JE, Zhang X (2005) Multidecadal variability of North Atlantic temperature and salinity during the Twentieth Century. J Clim 18:4562–4581

Rayner NA, Parker DE, Horton EB, Folland CK, Alexander LV, Rowell DP, Kent EC, Kaplan A (2003) Global analyses of sea surface temperature, sea ice, and night marine air temperature since the late nineteenth century. J Geophys Res 108(D14):4407. https://doi.org/10.1029/2002JD002670

Reick CH, Raddatz T, Brovkin V, Gayler V (2013) Representation of natural and anthropogenic land cover change in MPI-ESM. J Adv Model Earth Syst 5:459–482. https://doi.org/10.1002/jame.20022

Ruprich-Robert Y, Msadek R, Castruccio F, Yeager S, Delworth T, Danabasoglu G (2017) Assessing the climate impacts of the observed Atlantic Multidecadal Variability using the GFDL CM2.1 and NCAR CESM1 global coupled models. J Clim 30:2785–2810

Ruprich-Robert Y et al (2021) Impacts of Atlantic multidecadal variability on the tropical Pacific: a multi-model study. Npj Clim Atmos Sci 4:33

Stevens B, Giorgetta M, Esch M, Mauritsen T, Crueger T, Rast S, Salzmann M, Schmidt H, Bader J, Block K, Brokopf R, Fast I, Kinne S, Kornblueh L, Lohmann U, Pincus R, Reichler T, Roeckner E (2013) Atmospheric component of the MPI-M Earth System Model: ECHAM6. J Adv Model Earth Sy 5:146–172. https://doi.org/10.1002/jame.20015

Sun C, Li JP, Jin FF (2015) A delayed oscillator model for the quasi-periodic multidecadal variability of the NAO. Clim Dyn 45:2083–2099

Svendsen L, Hetzinger S, Keenlyside N, Gao Y (2014) Marine-based multiproxy reconstruction of Atlantic multidecadal variability. Geophys Res Lett 41:1295–1300

Tandon NF, Kushner PJ (2015) Does external forcing interfere with the AMOC's influence on north atlantic sea surface temperature? J Clim 28(16):6309–6323. https://doi.org/10.1175/JCLI-D-14-00664.1

Toohey M, Sigl M (2017) Volcanic stratospheric sulfur injections and aerosol optical depth from 500 BCE to 1900 CE. Earth Syst Sci Data 9:809–831. https://doi.org/10.5194/essd-9-809-2017

Torrence C, Compo GP (1998) A practical guide to wavelet analysis. Bull Am Meteor Soc 79:61–78

Waite AJ, Klavans JM, Clement AC, Murphy LN, Liebetrau V, Eisenhauer A, Weger RJ, Swart PK (2020) Observational and model evidence for an important role for volcanic forcing driving Atlantic Multidecadal Variability over the last 600 years. Geophys Res Lett 43:e2020GL089428. https://doi.org/10.1029/2020GL089428

Watanabe M, Tatebe H (2019) Reconciling roles of sulphate aerosol forcing and internal variability in Atlantic multidecadal climate changes. Clim Dyn 53:4651–4665

Wessel P, Smith WHF (1996) A global, self-consistent, hierarchical, high-resolution shoreline database. J Geophys Res Solid Earth 101:8741–8743. https://doi.org/10.1029/96JB00104

Winter A, Zanchettin D, Miller T, Kushnir Y, Black D, Lohmann G et al (2015) Persistent drying in the tropics linked to natural forcing. Nat Commun 6:7627. https://doi.org/10.1038/ncomms8627

Wu S, Liu Z, Zhang R, Delworth TL (2011) On the observed relationship between the Pacific decadal oscillation and the Atlantic multi-decadal oscillation. J Oceanogr 67:27–35. https://doi.org/10.1007/s10872-011-0003-x

Yan X, Zhang R, Knutson TR (2019) A Multivariate AMV index and associated discrepancies between observed and CMIP5 externally forced AMV. Geophys Res Lett 47:4421–4431. https://doi.org/10.1029/2019GL082787

Yeager S (2015) Topographic coupling of the Atlantic overturning and gyre circulations. J Phys Oceanogr 45:1258–1284. https://doi.org/10.1175/JPO-D-14-0100.1

Zanchettin D, Rubino A, Jungclaus JH (2010) Intermittent multidecadal-to-centennial fluctuations dominate global temperature evolution over the last millennium. Geophys Res Lett 37:L14702. https://doi.org/10.1029/2010GL043717

Zanchettin D, Rubino A, Matei D, Bothe O, Jungclaus JH (2013) Multidecadal-to-centennial SST variability in the MPI-ESM simulation ensemble for the last millennium. Clim Dyn 40(5):1301–1318. https://doi.org/10.1007/s00382-012-1361-9

Zanchettin D, Bothe O, Müller W, Bader J, Jungclaus JH (2014) Different flavors of the Atlantic Multidecadal Variability. Clim Dyn 42(1–2):381–399. https://doi.org/10.1007/s00382-013-1669-0

Zanchettin D, Bothe O, Rubino A, Jungclaus JH (2016a) Multi-model ensemble analysis of Pacific and Atlantic SST variability in unperturbed climate simulations. Clim Dyn 47(3):1073–1090. https://doi.org/10.1007/s00382-015-2889-2

Zanchettin D, Bothe O, Graf HF, Omrani N-E, Rubino A, Jungclaus JH (2016b) A decadally delayed response of the tropical Pacific to Atlantic multidecadal variability. Geophys Res Lett 43:784–792. https://doi.org/10.1002/2015GL067284

Zanchettin D, Timmreck C, Toohey M, Jungclaus JH, Bittner M, Lorenz SJ, Rubino A (2019) Clarifying the relative role of forcing uncertainties and initial-condition unknowns in spreading the climate response to volcanic eruptions. Geophys Res Lett. https://doi.org/10.1029/2018GL081018

Zhang R (2017) On the persistence and coherence of subpolar sea surface temperature and salinity anomalies associated with the atlantic multidecadal variability. Geophys Res Lett 44:7865–7875. https://doi.org/10.1002/2017GL074342

Zhang R et al (2013) Have aerosols caused the observed Atlantic multidecadal variability? J Atmos Sci 70:1135–1144. https://doi.org/10.1175/JAS-D-12-0331.1

Zhang R, Sutton R, Danabasoglu G, Delworth TL, Kim WM, Robson J, Yeager SG (2016) Comment on "The Atlantic Multidecadal Oscillation without a role for ocean circulation." Science 352:1527. https://doi.org/10.1126/science.aaf1660

Publisher's Note Springer Nature remains neutral with regard to jurisdictional claims in published maps and institutional affiliations.

Springer Nature or its licensor (e.g. a society or other partner) holds exclusive rights to this article under a publishing agreement with the author(s) or other rightsholder(s); author self-archiving of the accepted manuscript version of this article is solely governed by the terms of such publishing agreement and applicable law.